ACS OMEGA

Open Access

http://pubs.acs.org/journal/acsodf

Article

Organic Geochemistry and 1-D Basin Modeling of the Late Triassic Baluti Formation: Implication of Shale Oil Potential in the Kurdistan Region of Iraq

Ibrahim M. J. Mohialdeen, Mohammed Hail Hakimi,* Sardar S. Fatah, Rzger A. Abdula, Polla A. Khanaqa, Mahdi Ali Lathbl, and Waqas Naseem

Cite This: *ACS Omega* 2024, 9, 7085−7107

Read Online

ACCESS | Metrics & More | Article Recommendations

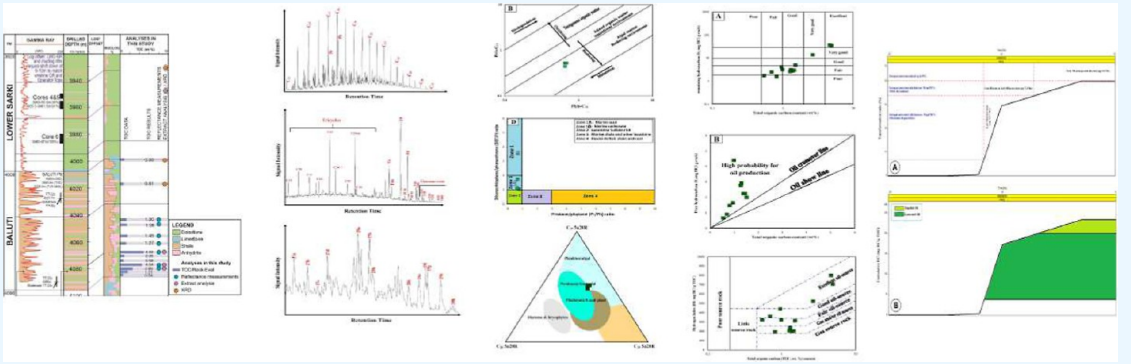

ABSTRACT: This investigation looks at the Late Triassic Baluti Formation's organic geochemical, mineralogical, and petrographical characteristics from a single exploration well (TT-22) near the Taq Taq oilfield in northern Iraq. The Baluti Formation shale samples that were studied in the studied well have high total organic carbon (TOC %) values up to 4.92 wt % and mostly hydrogen-rich types I and II kerogen with a minor gradient to types II/III and III kerogen, indicating a good oil-source rock. The hydrogen-rich kerogen was also confirmed by various organic matter (OM) origins and depositional environment-related biomarkers. The biomarker indicators demonstrate that the Baluti shale was deposited under anoxic conditions and contains a variety of OM generated mostly from algae marine and other aqueous organic materials, along with some terrigenous land plants. The geochemical and optical maturity indicators show that most of the examined Baluti shale samples, with a deep burial depth of more than 4000 m, are thermally mature, thus defining peak-mature to late-mature stages of the oil generation window. According to the basin models, from the late Miocene to the present, between 10 and 59% of the kerogen in the Baluti shale source rock has been transformed into oil, which is consistent with the VR values between 0.77 and 1.08%. The presence of the oil crossover in these shale rocks with an oil saturation index of more than 100 mg HC/g rock supports the maximal oil generation from the Baluti source rock system. Additionally, there was little oil expulsion from the Baluti source rock system at the end of the late Miocene, with transformation ratio values below 60% (59%). Considering the more significant oil generation and little expulsion, a high pressure was generated and forced the brittle minerals of the Baluti shales (mainly quartz), creating a natural fracture system as recognized and observed in the thin section. This natural fracture system enhances the porosity system of tight shale rocks of the Baluti Formation, giving rise to a high probability of oil production using hydraulic fracturing stimulation.

1. INTRODUCTION

Petroleum resources have received increased attention, such that shale oil- and shale gas resources have recently become important global exploration targets.[1] Marine and continental organic-rich shale rocks have been successfully explored and developed worldwide, showing remarkable potential in any sedimentary basin.[2,3] Multi-integrated techniques are vital to the study of shale oil systems, where organic geochemistry and microscopic examination combined with 1-D basin modeling can be used to evaluate the organic matter (OM) characteristics, their ability to generate oil, and their recoverable estimates in sedimentary basins.[4,5]

Received: November 14, 2023
Revised: December 31, 2023
Accepted: January 8, 2024
Published: January 31, 2024

https://doi.org/10.1021/acsomega.3c09003
ACS Omega 2024, 9, 7085−7107

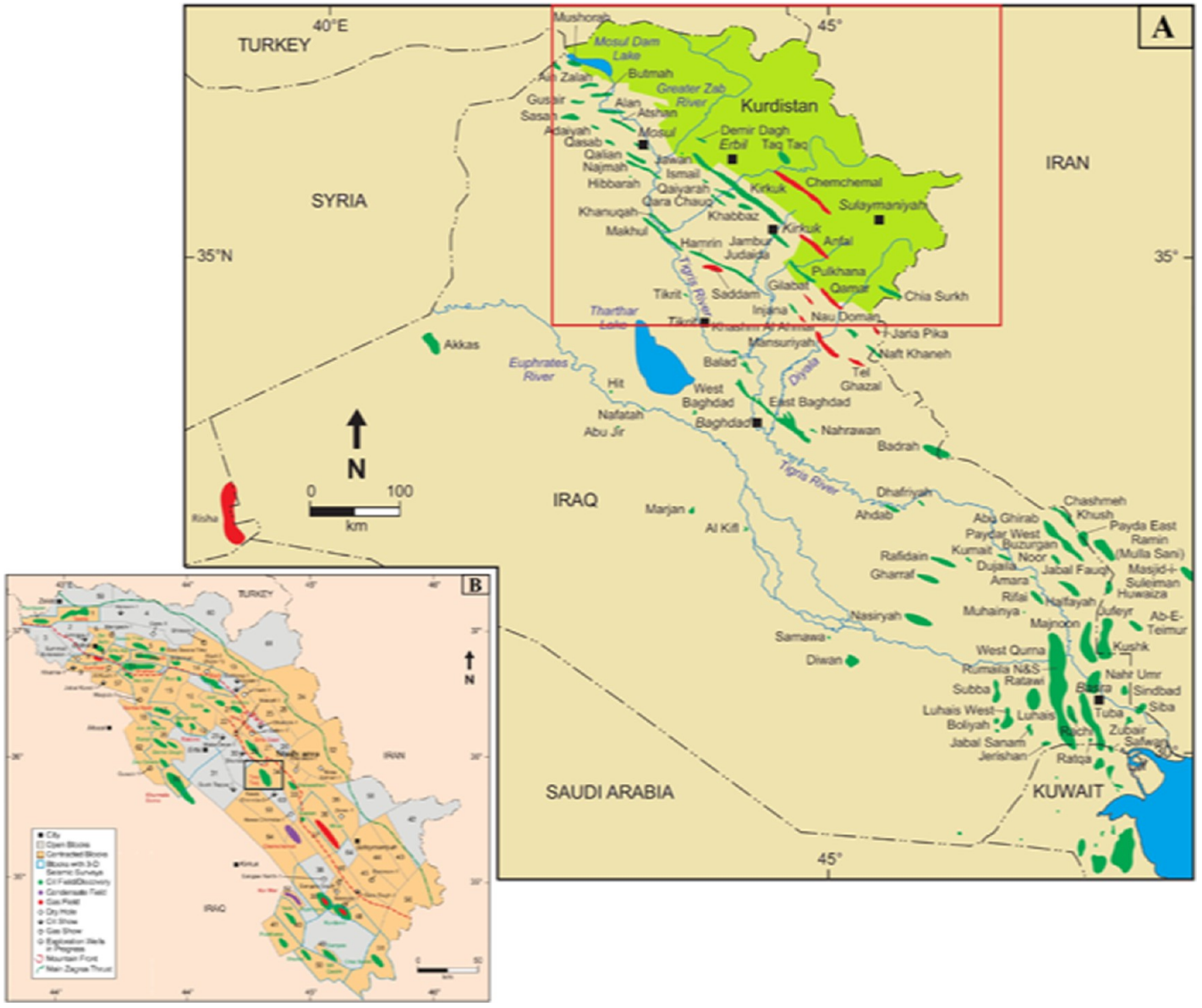

Figure 1. (A) Location map for the northeast Arabian Peninsula in Iraq, which shows ZFB with oil and gas field locations, including studied oil field location (B).

The key focus of the present study is the Zagros Fold Belt (ZFB), which runs northwest-southeast in the northern part of the country (Figure 1a). The ZFB of the northern part of Iraq is one of the biggest and oldest oil-producing zones in Iraq and has seen oil production from oil fields of more than 15 various sizes (Figure 1b). Due to its good source rock appearances and the discovery of commercial petroleum accumulations in the basin, the ZFB has attracted the attention of the scientific community and the oil industry. Numerous investigations regarding the geochemical characteristics of the organic-rich Mesozoic sedimentary rock units have clarified the presence of excellent source rock intervals in the Jurassic and Cretaceous rock units.[6−14] The most important and well-known ones are the Sargelu carbonates (Middle Jurassic), the Naokelekan carbonates and shales (Late Jurassic), and the Chia Gara carbonate-rich rocks (Late Jurassic-Early Cretaceous).[10−12,15,16] Most of these formations in the northern Iraq's oilfields, especially the Sargelu Formation, are filled with high-bituminous carbonate-rich rocks and reached a higher burial depth than other formations.[13] The ZFB in northern Iraq's Sargelu Formation is thought to be the primary source rock in this instance.[8,14] The types I and II kerogens and mixed type II/III kerogens in the Sargelu organic-rich carbonates, which were deposited in a marine environment, make primarily oil-prone source rocks.[6,13] Good geochemical relationships between the reservoir oils and the mature Sargelu rocks in the basin support this discovery.[8] The Sargelu Formation is the main oil-source rock and is directly related to the main petroleum-producing regions recognized to date, acting as a conventional petroleum resource, according to Hakimi and Najaf[8] analysis of the biomarker fingerprints of reservoir oils from oilfields in the ZFB. There is only one oil family, and the Sargelu Formation is acting as a conventional petroleum resource.

Although the majority of earlier studies suggested that the organic-rich carbonate rocks of the Sargelu Formation are an important source rock potential for conventional exploration and production targets in northern Iraq, little is known about the organic-rich shales within the Late Triassic succession, particularly those from the Late Triassic Baluti Formation (Figure 2), which is the main subject of this investigation.

The Late Triassic Baluti Formation's organically rich shale intervals from the TT-22 well in the Taq Taq oilfield in Iraqi

https://doi.org/10.1021/acsomega.3c09003
ACS Omega 2024, 9, 7085−7107

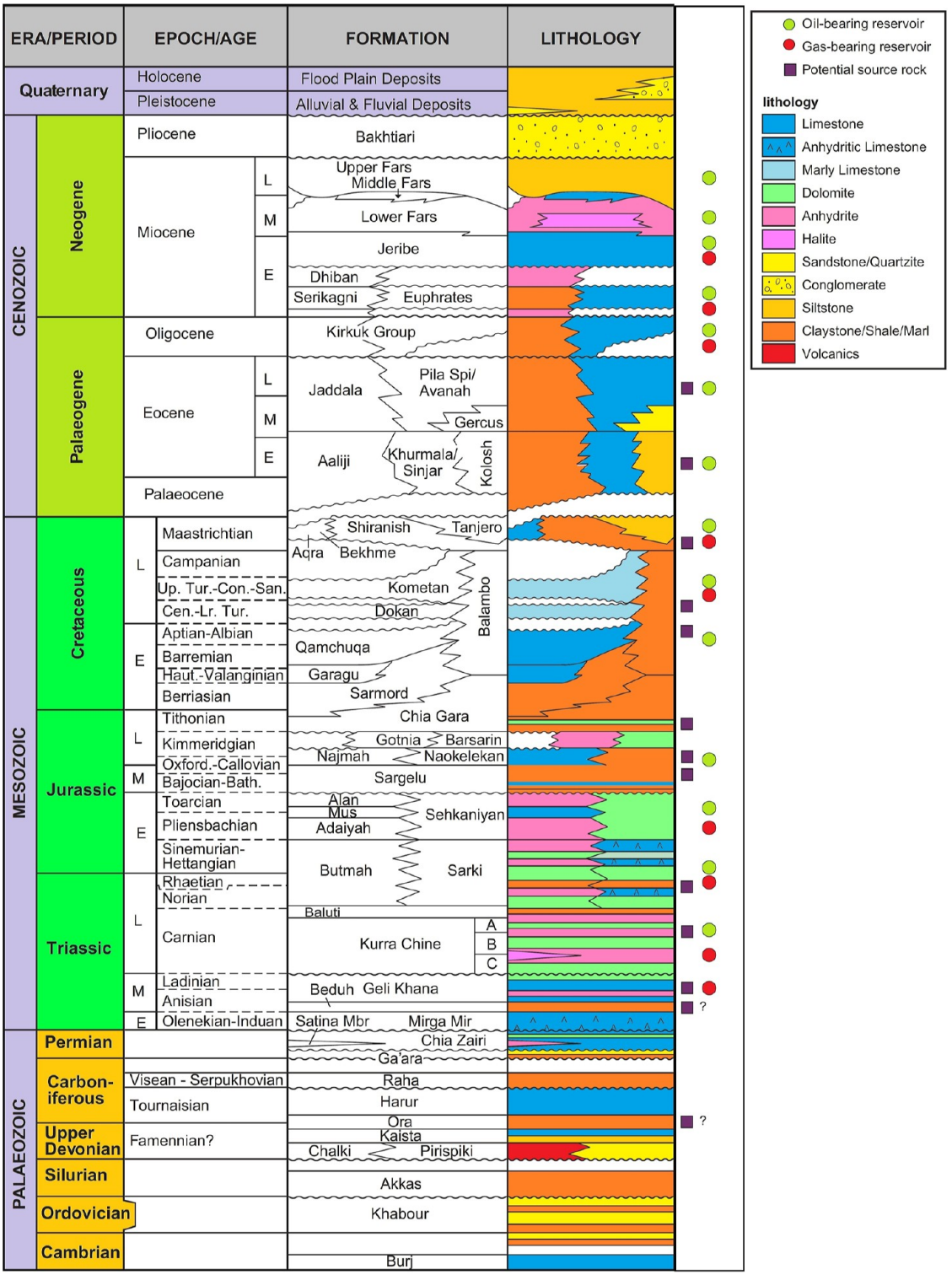

Figure 2. Stratigraphic correlation chart for the Iraq and Kurdistan area, showing the Paleozoic-Cenozoic successions and the hydrocarbon occurrences.

Kurdistan were thoroughly examined in this article, including their organic geochemistry, mineralogy, and petrographical features.

This study's objectives were to determine the OM content, identify the present kerogen types, assess the petroleum generation potential, assess the OM's origin, and prevail environmental conditions during deposition by employing multiple biomarkers. In order to anticipate the geothermal history, the ratios of the kerogen's transformation into oil, the stages of oil production, and the expulsion of the Baluti source rock system, organic geochemical results are integrated with basin modeling and utilized to determine the potential of shale oil. This study also addresses the role of the petrographic data from an X-ray diffraction (XRD) experiment and a thin-section microscope in characterizing the types of visible porosity and mineralogical composition.

https://doi.org/10.1021/acsomega.3c09003
ACS Omega 2024, 9, 7085−7107

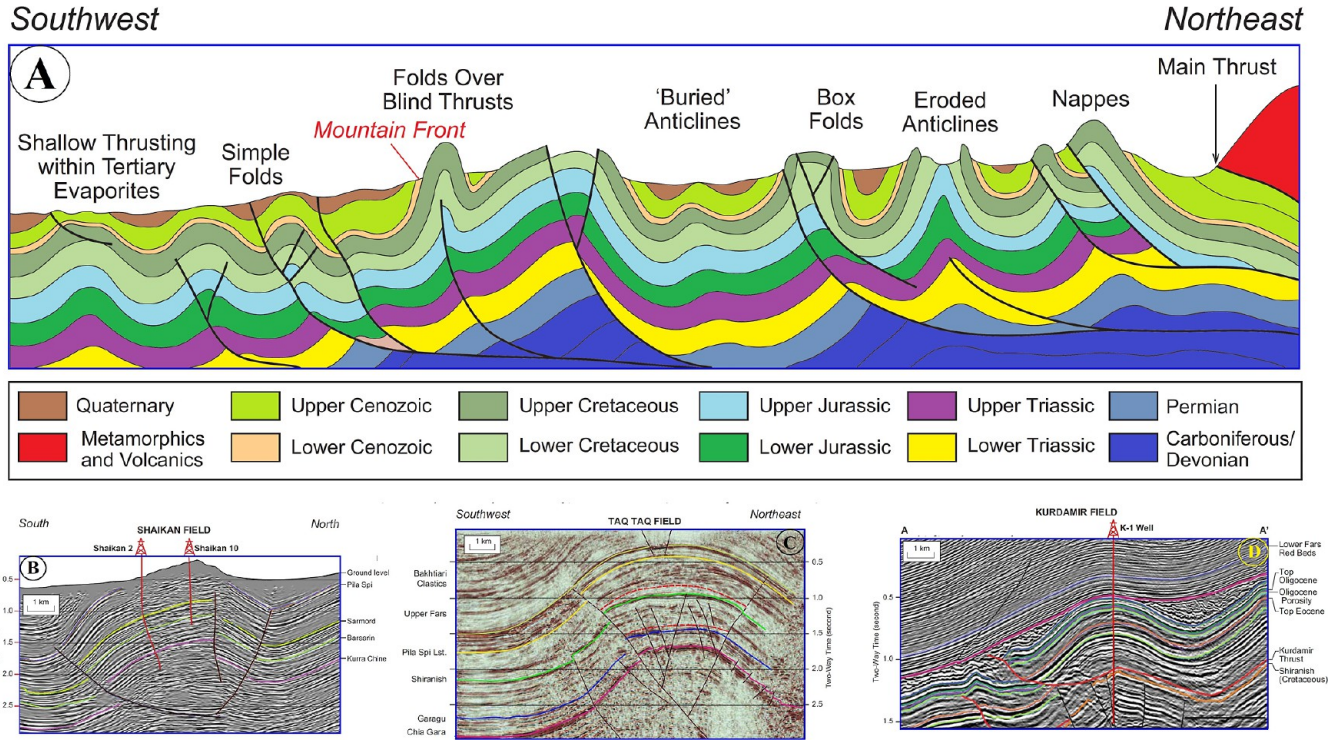

Figure 3. (A) Northwest-southeast structural cross-section across ZFB in north Iraq, indicating structures and lithology of rock units. (B) Seismic cross-section in the Shaikan oil field. (C) Seismic cross-section in the Taq Taq oil field. (D) Seismic cross-section in the kurdamir oil field (for location, see Figure 1B).

2. GEOLOGICAL SETTING

On the northeastern edge of the Arabian Plate, North Iraq is located inside the Zagros Fold-Thrust Belt (Figure 1a). The Arabian and Eurasia plates collided throughout the Cretaceous and Tertiary periods, resulting in the formation of the Zagros Mountains.[17−20] Thrust belt marks the collision zone between the Arabian and Eurasian plates, which extends through SE Turkey, NE Iraq, and western Iran.[21,22] When the Neo-Tethys reached its maximum width of 4000 km in the Late Triassic to Middle Jurassic periods, the second stage of opening began.[23,24] Throughout the Middle Triassic and Late Triassic, new extensions developed on the Arabian Plate's northern and eastern edges.[25] The associated tectonic activity produced a thick sedimentary fill in the foreland basin depocenter (resulting in the maturation of underlying source rocks) and the formation of large anticline folds (that have trapped the generated oil) (Figure 3a), making the ZFB of northern Iraq a prolific region of structural trapping for hydrocarbon production (Figure 3b−d; Mackertich and Samarra[26]).

The lithostratigraphic column of the Kurdistan region, ranging from northern to northeastern Iraq is presented in Figure 2 of Mackertich and Samarra.[26] The Kurdistan region received a mixture of clastic, carbonate, and evaporite sediments ranging from the Paleozoic (Cambrian-Permian) to the Cenozoic (Paleocene-Pliocene), with the maximum thickness of the Mesozoic (early Triassic-Late Cretaceous) sedimentary succession (Figure 2). The Mesozoic sediments are mostly carbonate, shale, and anhydrite deposited in marine to lagoonal shelf settings.[27] The Baluti Formation, the primary subject of this investigation, is composed of carbonate-evaporate and subsidiary shale sequences (Figure 2), with its complementary type-section located near Sarki Village, Kurdistan region in North Iraq, near the middle of the Gara anticline.[27] The Baluti Formation was mostly deposited in a lagoonal estuary environment,[27] and the neritic lagoonal and evaporitic episodes of the depositional environment were also identified based on palynology and sedimentology investigations.

3. DATASETS AND METHODS

In the current study, detailed organic geochemical, petrographic, and mineralogical analyses were performed on cutting samples from one exploration well (TT-22) in the Taq Taq oilfield of the ZFB, northern Iraq (Figure 1a). These cutting samples were collected from the calcareous shale intervals with high gamma ray responses at different depths (4008−4096 m) of the Late Triassic Baluti Formation (Figure 4). A higher gamma-ray response in the shales of the thicker Baluti Formation may reflect a deeper deposition environment and potentially more organic-rich facies. However, the studied well was drilled using water-based mud; therefore, the collected cutting samples were mainly washed with cold water to remove the mud drilling before being subjected to multi-geochemical and optical analyses.

The description of the organic geochemical and petrographic analyses along the 1-D basin modeling study is highlighted in the next subsections.

3.1. Organic Geochemical Analyses. Thirteen calcareous shale samples from the Baluti Formation were analyzed for total organic carbon (TOC) content (TOC %) and conventional programmed pyrolysis (Rock-Eval 6). To remove carbonate minerals from the original crushed samples, 10% diluted HCl was used. 100 mg of the cleaned crushed samples was then tested using the Rock-Eval (RE) pyrolysis (Rock-Eval 6) apparatus to ascertain the TOC % content and the bulk programmed pyrolysis results.

In an atmosphere of helium, the samples were heated to 600 °C. After maintaining 300 °C for three min, the oven's

https://doi.org/10.1021/acsomega.3c09003
ACS Omega 2024, 9, 7085−7107

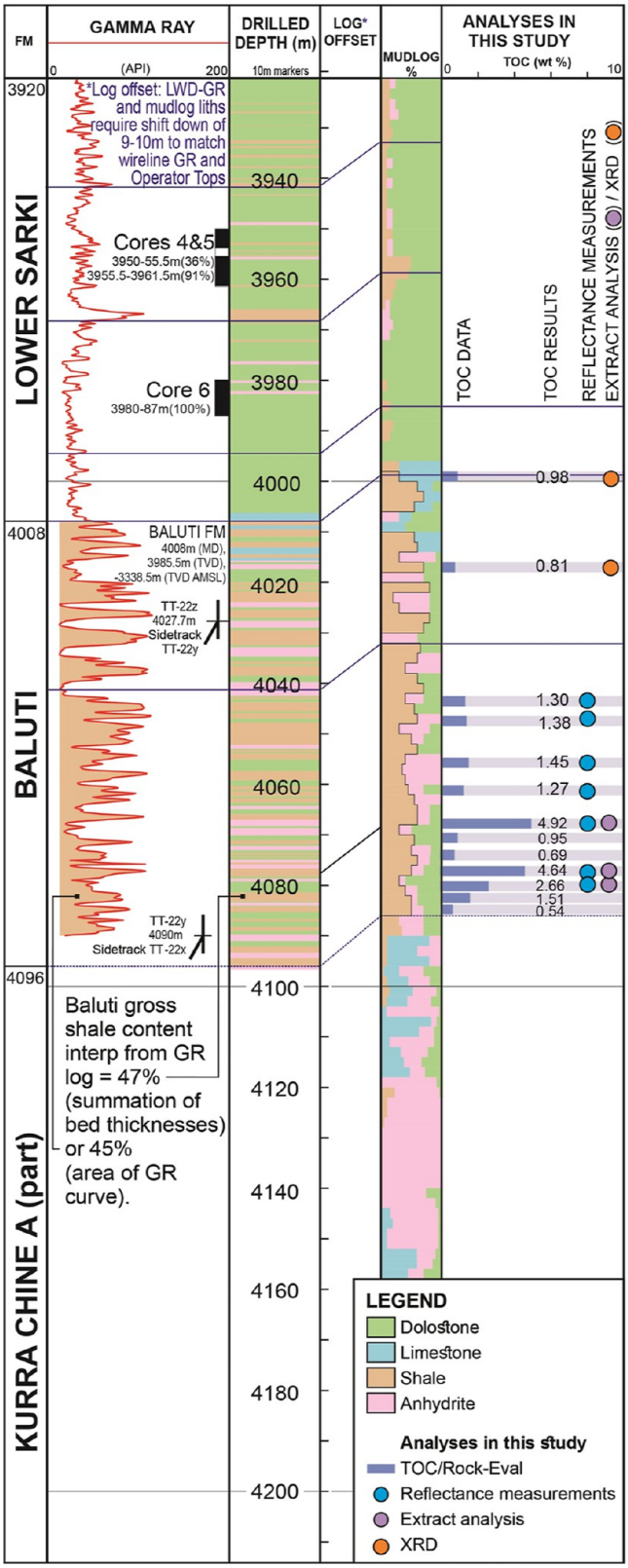

Figure 4. Stratigraphic column of Baluti and Lower Sarki Formations from TT-22 well, Kurdistan region, northern Iraq, and the location of studied samples with different geochemical techniques used in this study.

temperature was raised by 25 °C every minute. The characteristics that are evaluated during pyrolysis comprise TOC % content, pyrolysis yields of S_1, S_2, and S_3, and the maximum temperature (T_{max}) of S_2 production (Table 1). According to Peters and Cassa,[28] several other limitations, including the hydrogen index (HI = $S_2 \times 100$/TOC), oxygen index (OI = $S_3 \times 100$/TOC), and production index (PI = $S_1/S_1 + S_2$), were also determined using various RE yields.

3.2. Organic Petrological Analysis. In this study, organic petrographic examinations were performed on seven shale samples, with more than 1 wt % TOC, in order to identify the organic facies in the studied samples along with vitrinite reflectance (% VRo) measurements by means of the standard polished block method.[29] The whole samples were ground up ∼2−3 mm and placed in molds using a blend of Serifix resin and cold mount hardener. Once hardened, the block was pulverized to expose the sample surface and then individually polished to smooth surfaces following ASTM D2797−04.[30]

The vitrinite reflectance (VRo) in polished blocks was measured with a 50x oil immersion objective using a plane-polarized reflected-light LEICA DM 6000 M microscope supplied with Diskus Fossil software. The calibration was performed using a piece of sapphire glass standard with a reflectance value of 0.589%, and the numbers presented were the arithmetic means of 10−30 measurements (Table 1). Although the number of vitrinite measurements is relatively low for some samples, the standard deviation values of the measurement are around 0.05−0.12 (Table 1), and these low values of the standard deviation are normally acceptable. Thus, the VRo measurements of the analyzed samples are reliable.

3.3. Bitumen Extraction and Gas Chromatography-Mass Spectroscopy (GC-MS). Three representative samples were selected based on TOC of more than 2 wt % and then subjected to extraction. The soluble bitumen (expressed in ppm of the total rock sample) in these samples was extracted through the blended solvents of dichloromethane (DCM) and methanol (CH_3OH) for 3 days (72 h). The extracted bitumen from these three samples was fractionated into three fractions; aliphatic, aromatic hydrocarbons, and polar compounds (NSO) by means of petroleum ether, DCM, and CH_3OH solvents, respectively, in liquid column chromatography (LCQ) with alumina and silica gel.

The three studied materials' aliphatic and aromatic fractions were then subjected to GC-MS analysis utilizing an HP 5975B MSD-fused silica capillary column with a 30 m length, 0.25 μm inner diameter, and 0.25 μm film thickness, along with helium as the carrier gas. The Flame Ionization Detector's temperature gradually increases from 40 to 300 °C at a consent rate of 4 °C/min and then was held for 30 min at 320 °C.

Tricyclic terpanes, hopanes, steranes, and diasteranes, as well as their proportions and characteristics, were evaluated using GC-MS analysis using specific ions such as m/z 191 and 217 mass fragmentograms. The heterocyclic and polycyclic aromatic compounds in the aromatic HC fraction were also produced from the GC-MS and studied based on specific ions, e.g., m/z 170, 178, 184, 192, and 198 mass fragmentograms. However, peak identification was established by comparing the studied ion's retention time and mass spectra with those previously published.[31−33]

3.4. Thin-Section Microscopy and X-ray Diffraction Analysis. In this work, standard petrographic analysis, including thin sections and XRD, was utilized to estimate the visual porosity and mineral composition in the investigated Baluti shale samples. A standard thin-section examination was performed on four shale samples at the laboratories of the University of Sulaimani, Kurdistan, Iraq. In this case, visible

https://doi.org/10.1021/acsomega.3c09003
ACS Omega 2024, 9, 7085−7107

Table 1. Geochemical and Optical Results of the Analyzed Shales from the Late Triassic Baluti Formation in the TT-22 Well in the Taq Taq Oilfield, Including TOC Content, Solid Bitumen, RE Pyrolysis, and Reflectance Measurements of Bitumen-Stained Vitrinite OM (% VRo)[a]

				Rock-Eval pyrolysis data									VRo (%)		
sample ID	depth (m)	TOC (wt %)	solid bitumen (ppm)	S_1–HC (mg/g)	S_2–HC (mg/g)	S_3–CO^2 (mg/g)	HI (mg/g)	OI (mg/g)	PY (mg/g)	PI (mg/g)	T_{max} (°C)	OSI (mg/g)	mean	number measuring	SD
TT1	4009	0.98		4.40	3.14	0.52	320	53	7.54	0.58	301	448.98			
TT2	4027	0.81		1.47	1.55	0.51	191	63	3.02	0.49	307	181.48			
TT3	4053	1.30		2.94	3.09	1.84	238	142	6.03	0.49	391	226.15	1.02	25	0.10
TT4	4059	1.38		2.24	2.75	2.48	199	180	4.99	0.45	394	162.32	0.97	10	0.05
TT5	4065	1.45		2.24	2.95	2.41	203	166	5.19	0.43	400	154.48	0.92	10	0.06
TT6	4071	1.27		2.77	2.59	2.19	204	172	5.36	0.52	395	218.11	1.07	20	0.07
TT7	4077	4.92	9572.95	6.77	34.74	4.00	706	81	41.51	0.16	394	137.60	1.06	30	0.10
TT8	4079	0.95		1.65	4.16	0.76	438	80	5.81	0.28	397	173.68			
TT9	4081	0.69		0.92	2.48	0.65	359	94	3.40	0.27	426	133.33			
TT10	4083	4.64	10483.95	6.71	37.06	2.96	799	64	43.77	0.15	396	144.61	1.15	15	0.06
TT11	4089	2.66	6208.86	6.46	13.83	2.74	520	103	20.29	0.32	390	242.86	1.00	10	0.12
TT12	4091	1.51		2.00	4.90	0.79	312	50	6.90	0.29	395	132.45			
TT13	4093	0.54		0.68	1.73	0.40	320	74	2.41	0.28	436	125.93			

[a]TOC = total organic carbon; S_1-peak = free contents of hydrocarbon (mg HC/g rock); S_2-peak = remaining hydrocarbon potential (mg HC/g rock); S_3 peak = produced carbon dioxide (mg CO_2/g rock); HI = hydrogen index [$S_2 \times 100$/TOC (mg HC/g rock)]; OI = oxygen index [$S_3 \times 100$/TOC (mg CO_2/g TOC)]; T_{max} = maximum temperature at peak of S_2 (°C); PI = production index [S_1/($S_1 + S_2$)]; OSI = oil saturated index (S_1*100/TOC); and VR = measured vitrinite reflectance.

https://doi.org/10.1021/acsomega.3c09003
ACS Omega 2024, 9, 7085−7107

http://pubs.acs.org/journal/acsodf

Table 2. Basin Model Input Data Used to Reconstruct the Burial and Thermal History One Well Location (TT-22) in the Taq Taq Oilfield, As Shown in Figure 1B

		deposition ages (Ma)		erosion ages (Ma)			TT-22 well		
formation	lithology	from	to	from	to	erosion thickness (m)	top (m)	bottom (m)	thickness (m)
Injana (Upper Fars)	sandstone, claystone	12	3	3	0	2900	10	269	259
Fatha (Lower Fars)	limestone, sandstone, evaporite	19	12				269	553	284
Pila Spi	limestone	43	34	34	19	50	553	675	122
Gercus	sandstone, claystone	47	43				675	731	56
Khurmala	limestone, dolomite	52	51	51	47	30	731	781	50
Sinjar	limestone, dolomite	54	52				781	890	109
Kolosh	sandstone, shale	65	54				890	1624	734
Tanjero	sandstone, marl, argillaceous limestone	67	66				1624	1675	51
Shiranish	limestone, marl	78	67				1675	2062	387
Kometan	limestone	92	78				2062	2189	127
Gulneri	limestone, claystone	93	92				2189	2190	1
Dokan	limestone	97	93				2190	2204	14
Mauddud (UQamchuqa)	limestone, dolomite	109	100	100	97	20	2204	2418	214
Batiwah (NUmr Eq.)	limestone, dolomite	113	109				2418	2478	60
M Qamchuqa Lst Eq	limestone, dolomite	129	120	120	113	130	2478	2581.5	103.5
Garagu	limestone	134	129				2581.5	2662	80.5
Sarmord	limestone, marl	143	134				2662	3078	416
Chia Gara	limestone, shale	152	143				3078	3172	94
Barsarin	limestone, dolomite, evaporite	155	152				3172	3236	64
Naokelekan	limestone, shale	164	155				3236	3256	20
Sargelu	limestone, shale	170	164				3256	3362	106
Alan	limestone, evaporite	180	177				3362	3457	95
Mus	limestone	184	180				3457	3493	36
Adaiyah	limestone, evaporite	194	184				3493	3552	59
Upper Sarki Mb	limestone, evaporite	201	194				3552	3758	206
Middle Sarki Mb	limestone	222	203				3758	3920	162
Lower Sarki Mb	limestone	228	226.5				3920	4008	88
Baluti	shale, dolomite, anhydrite, limestone	229	228				4008	4096	88
Kurra Chine A	anhydrite, dolomite	232	229				4096	4214	118
Kurra Chine B	shale, anhydrite, dolomite	236	232				4214	4466	252
Kurra Chine C Anhy (approx)	anhydrite, dolomite, limestone	237	236				4466	4613.5	147.5+
total depth							4613.5		

porosity and pore types were estimated by using the image analysis on thin-section photomicrographs.

The Baluti shale samples were also studied using XRD analysis and used to reveal the qualitative and quantitative mineralogical compositions of the Baluti shale. XRD analysis was also carried out on three samples of the Baluti formation from the studied well (TT-22) using a Malvern PANalytical XRD diffractometer (XPERT-ROP diffractometer) using monochromatic—CuKα1 radiation (λ = 1.540598 Å).

3.5. Basin Modeling Procedures. The geological and thermal maturity data (i.e., VRo) were imported into Schlumberger's PetroMod 1-D modeling software (version 2010 SP1) and used to build burial and thermal history models of the Late Triassic Baluti source rock system. In this example, a single exploratory well (TT-22) drilled to a total depth of up to 4613 m (Table 2) was utilized to construct basin models for the Late Triassic succession's thermal history progression.

Geological information, including sedimentary rock types and deposition and erosion periods, was obtained from the TT-22 well's private well log record (Table 2), and the age of deposition and erosion periods was derived from the stratigraphic data available in the published literature.[34,35] A significant thickness of sediments, around 1500 m to more than 4000 m, was eroded throughout Late Cretaceous-Pliocene time.[8,35,36] These nearby estimations of eroded sediments were integrated into the basin modeling study (Table 2). For the purpose of estimating the thermal history of sedimentary basins over time, which impacts the maturity of the source rock, heat flow (HF) and temperature gradient are crucial input parameters.[37−41] Theoretically, heat produced by local hydrodynamic fluxes and crustal tectonic processes caused the HF to form in the mantle.[42−44] The HF is a more severe indicator of the thermal evolution in any basin since the ancient HF was inferred from key tectonic events, especially the extensional tectonics of the rifting epoch.[41,44]

The maturity data from measured % VRo and maximum temperature (T_{max}) can all be used to estimate the paleo-HF.[37,43,44] This maturity calibration data was used to establish the paleo-HF and entire thermal maturity history for the sedimentary sequence within the sedimentary basins.[45−51]

In this study, the % VRo values, as demonstrated in Table 2, were used to calibrate the evolution of geothermal maturation for the studied well utilizing the Easy % Ro method, devised by Sweeney and Burnham.[52] This model has good agreement with

https://doi.org/10.1021/acsomega.3c09003
ACS Omega 2024, 9, 7085−7107

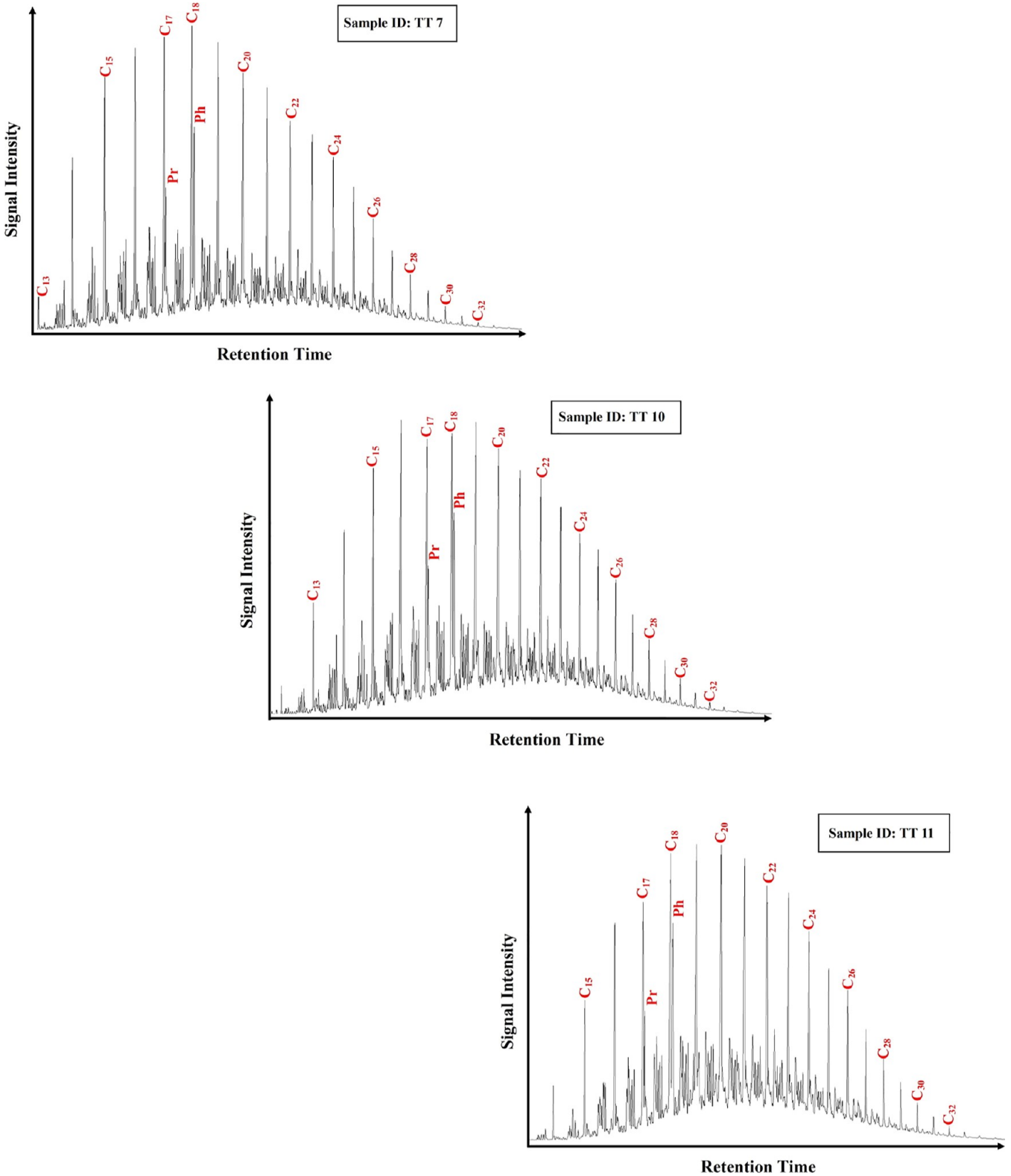

Figure 5. *m*/*z* 85 mass fragmentograms show *n*-alkane and acyclic isoprenoid (e.g., pristane and phytane) distributions of the aliphatic hydrocarbon fraction in the representative organic-rich shale samples of the Baluti Formation.

the measured VRo data and the Easy % Ro model using the Petro Mod basin modeling program.

4. RESULTS

4.1. Vitrinite Reflectance Results. The maturation of the Baluti shale samples and the evolution of the thermal history across the examined well section were both revealed by measuring the VRo.

https://doi.org/10.1021/acsomega.3c09003
ACS Omega 2024, 9, 7085−7107

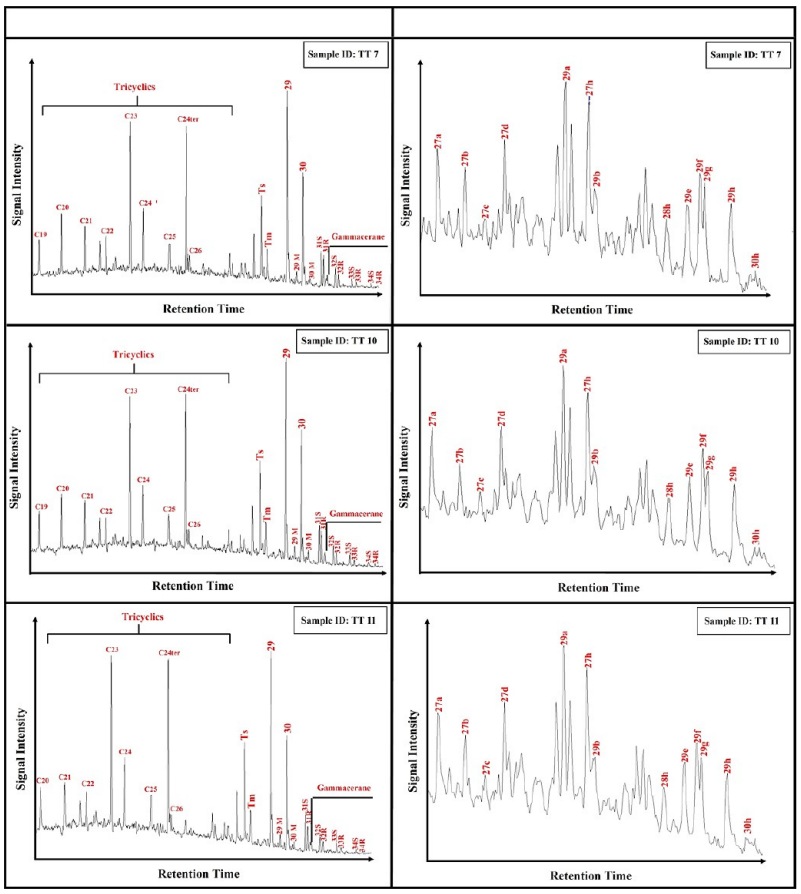

Peak assignments for hydrocarbons in the gas chromatograms of saturated fractions in the m/z 191 (I) and 217 (II) mass fragmentograms

(I) Peak *no.*	Compound abbreviation	
Ts	18α(H),22,29,30-trisnorneohopane	Ts
Tm	17α(H),22,29,30-trisnorhopane	Tm
29	17α,21β(H)-nor-hopane	C_{29} hop
30	17α,21β(H)-hopane	Hopane
30M	17 β,21α (H)-Moretane	C_{30}Mor
31S	17α,21β(H)-homohopane (22S)	C_{31}(22S)
31R	17α,21β(H)-homohopane (22R)	C_{31}(22R)
32S	17α,21β(H)-homohopane (22S)	C_{32}(22S)
32R	17α,21β(H)-homohopane (22R)	C_{32}(22R)
33S	17α,21β(H)-homohopane (22S)	C_{33}(22S)
33R	17α,21β(H)-homohopane (22R)	C_{33}(22R)
34S	17α,21β(H)-homohopane (22S)	C_{34}(22S)
34R	17α,21β(H)-homohopane (22R)	C_{34}(22R)
35S	17α,21β(H)-homohopane (22S)	C_{35}(22S)
35R	17α,21β(H)-homohopane (22R)	C_{35}(22R)
(II) Peak *no.*		
a	13β,17α(H)-diasteranes 20S	Diasteranes
b	13β,17α(H)-diasteranes 20R	Diasteranes
c	13α,17β(H)-diasteranes 20S	Diasteranes
d	13α,17β(H)-diasteranes 20R	Diasteranes
e	5α,14α(H), 17α(H)-steranes 20S	ααα20S
f	5α,14β(H), 17β(H)-steranes 20R	αββ20R
g	5α,14β(H), 17β(H)-steranes 20S	αββ20S
h	5α,14α(H), 17α(H)-steranes 20R	ααα20R

Figure 6. *m*/*z* 191 and 217 mass fragmentograms of the aliphatic hydrocarbon fraction in the representative organic-rich shale samples of the Baluti Formation.

The shale samples of the Baluti Formation are generally proven to be poor of vitrinite and are usually found as small size particles. However, most of the vitrinite materials are associated with bitumen staining, while other materials are unstained vitrinite. In this case, the unstained vitrinite is not indigenous OM and has been reworked from land plants. Accordingly, the VRo measurements of the selected samples were performed on bitumen-stained vitrinite OM as an indigenous OM. Thus, the VRo measurements are reliable as a thermal maturity indicator. The analyzed Baluti shale samples from well TT-22 have mean VRo values ranging from 0.92 to 1.15% (Table 1). These numbers generally show that the carbonate rocks from Baluti and Sarki, which are rich in solid bitumen, are indicative of a thermally mature sequence. The temperature burial of more than 4000 m is responsible for the high-maturity level in the succession of the Late Triassic Baluti Formation.

4.2. Bulk Geochemical Results. All shale samples from the Baluti Formation in the studied well were analyzed, and their RE pyrolysis results and TOC content were also measured (Table 1). The measured TOC is reported as a function of weight % and shows that the analyzed Baluti shale samples exhibit a TOC range of 0.54−4.92 wt %. Most of the measurements indicate TOC > 1 (1.27−4.92 wt %), while the other six samples have the lowest TOC, ranging between 0.54 and 0.98 wt % (Table 1).

As indicated in Table 1, the results of the RE pyrolysis comprise S_1, S_2, S_3, T_{max}, OI, PI, and HI. The range of petroleum output from cracking kerogen (S_2) is 1.55 to 37.06 mg HC/g rock (Table 1). Recalled three samples have the largest S_2 yields, ranging from 13.83 to 37.06 mg HC/g rock, whereas the majority of the analyzed samples (n = 10 samples) have S_2 values of <5 mg HC/g rock (1.55−4.90 mg HC/g rock) (Table 1). The results of free hydrocarbon yields (S_1) are substantial, ranging between 0.68 and 6.77 mg of HC/g of rock (Table 1). The S_1 values for most of the analyzed samples (n = 11) are more than 1 (1.47−6.77 mg HC/g rock). The other 2 samples show the lowest S_1 yields, between 0.68 and 0.92 mg HC/g rock (Table 1).

The agreement between the S_2 and S_3 values and the TOC content results in the generation of HI and OI (Table 1). The samples under study exhibit HI values between 191 and 799 mg of HC/g of TOC (Table 1). The majority of the analyzed samples (n = 9 samples) have high HI values of greater than 300 mg HC/g TOC, while the other four samples had the lowest HI values, between 191 and 238 mg HC/g TOC (Table 1).

In terms of the OI value, the analyzed samples from the studied well have varied values from 50 to 180 CO_2/g TOC (Table 1). The samples range in OI values ranging from 50 to 94 mg CO_2/g TOC for the lowest values and from 103 to 180 mg CO_2/g TOC for the highest values (Table 1).

The programmed pyrolysis study also included measuring the T_{max} values based on the S_2 peak. T_{max}, which denotes the temperature at which S_2 peak yield is obtained, is more accurate when S_2 levels are higher than 1 mg/g rock.[53,54] Accordingly, the most frequently examined shale samples' credible T_{max} values vary from 301 to 436 °C and contain S_2 values greater than 1 mg/g rock (Table 1).

4.3. Molecular and Biomarkers of OM. The present study examined OM characteristics based on *n*-alkanes, isoprenoids

https://doi.org/10.1021/acsomega.3c09003
ACS Omega 2024, 9, 7085−7107

(Figure 5), and sterane and terpane biomarker distributions utilizing mass fragmentograms of m/z 191 and 217 ions from the saturated fraction (Figure 6).

The alkanes between C_{13} and C_{33} are distributed unimodally in the GC, with an excess of short (C_{13}−C_{20}) to middle-chain (C_{21}−C_{26}) n-alkanes (Figure 5). Such a typical alkane distribution in the analyzed samples gave low carbon preference index (CPI) values between 0.95 and 0.99 (Table 3). The extent of waxiness (WI) was estimated and found to be between 0.70 and 0.78 from the examined shale samples (Table 3).

A significant amount of acyclic isoprenoid hydrocarbons, such as pristane (Pr) and phytane (Ph), are present in the chromatograms of the three samples that were under investigation (Figure 5). In the chromatograms of the analyzed samples (Figure 5), Ph was more prevalent of the acyclic isoprenoids than Pr, resulting in a Pr/Ph isoprenoid ratio of lower than 1 and ranges between 0.65 and 0.77 (Table 3). Isoprenoid ratios relative to n-alkane concentrations (C_{17}−C_{18}) were compared and measured, providing their Pr/n-C_{17} and Ph/n-C_{18} ratios in the range of 0.44−0.52 and 0.65−0.68, respectively (Table 3).

From mass fragmentograms of m/z 191 and 217 ions, respectively, in the saturated hydrocarbon compounds of GC-MS (Figure 6), hopanoids and steroids were generated, and their ratios and characteristics were calculated (Table 3).

The mass fragmentograms of the m/z 191 ions contain significant levels of pentacyclic and tricyclic terpanes (Figure 6a). The hopanoids consist of homohopane (C_{31}−C_{34}) components, C_{30} hopane, and C_{29} norhopane. The C_{29} norhopanes, however, are dominant over the C_{30} hopanes (Figure 6a), with C_{29} norhopane/C_{30} hopane ratio values greater than 1.40 (Table 3). These high ratios of C_{29}/C_{30} indicate carbonate-rich facies as likely source rocks.[55]

The homohopane distributions, in particular, are dominated by C_{31}, and when the carbon concentration in all samples rises, the proportion slowly declines (Figure 6a). In comparison, the homohopane C_{31}22R series is lower in abundance than the C_{30} hopane (Figure 6a), resulting in C_{31}22R homohopane/C_{30} hopane (C_{31}R/C_{30}H) ratios between 0.24 and 0.30 (Table 3). Substantial quantities of 17 α(H)-trisnorhopane (Tm) and 18 α(H)-trisnorneohopane (Ts) are present, yielding Ts/Tm values of 2.67−3.00 (Table 3). The biomarker maturity ratios of C_{32} 22S/(22R + 22S) and C_{30}M/C_{30}H were also calculated using the hopanoid distribution (Table 3).

Mass fragmentograms of m/z 191 are also revealing significant tricyclic terpane concentrations, ranging from C_{19} to C_{26} (Figure 6a). The tricyclic terpane biomarkers have been used to calculate several ratios, such as C_{22} tricyclic/C_{21} tricyclic (C_{22}T/C_{21}T), C_{23} tricyclic/C_{24} tricyclic (C_{24}T/C_{23}T), and C_{26} tricyclic/C_{25} tricyclic (C_{26}T/C_{25}T), as shown in Table 3. In addition, the gammacerane biomarker for the most analyzed samples is reported in low quantities in m/z 191 mass fragmentograms (Figure 6a), and its gammacerane/C_{30} hopane (G/C_{30}) index ranges from 0.10 to 0.20 (Table 3).

The m/z 217 mass fragmentograms also contained and identified the sterane and diasterane biomarkers (Figure 6b). In the saturated hydrocarbon, mass fragmentograms of m/z 217 often show a high abundance of steranes (Figure 6b). The C_{27}−C_{29} regular steranes are distinguished from the C_{29} and C_{28} regular steranes by the existence of a significant amount of regular sterane C_{27} (Figure 6b). The relative abundance of C_{27}, C_{29}, and C_{28} is estimated in the range of 47.83−51.11, 31.11−32.61, and 17.78−19.57%, respectively (Table 3). Several ratios,

Table 3. Biomarker Ratios of the Analyzed Three Representative Shale Samples from the Late Triassic Baluti Formation from the TT-22 Well in the Taq Taq Oilfield, Illustrating Source OM, Depositional Environment Conditions, and Thermal Maturity Indicators[a]

	Source OM and Depositional Environment Conditions															
								tricyclic terpanes						regular steranes (%)		
sample ID	Pr/Ph	Pr/C_{17}	Ph/C_{18}	WI	CPI	C_{29}/C_{30}	G/C_{30}	HCR_{31}/HC_{30}	C_{26TT}/C_{25TT}	C_{22TT}/C_{21TT}	C_{24TT}/C_{23TT}	DBT/Phen	C_{27}/C_{29} regular steranes	C_{27}	C_{28}	C_{29}
TT7	0.67	0.44	0.65	0.72	0.99	1.75	0.20	0.30	0.60	0.80	0.41	1.75	1.60	50.00	18.75	31.25
TT10	0.77	0.52	0.65	0.80	0.96	1.54	0.10	0.25	0.50	0.90	0.41	1.05	1.47	47.83	19.57	32.61
TT11	0.65	0.52	0.68	0.70	0.95	1.48	0.12	0.24	0.50	0.67	0.42	1.13	1.64	51.11	17.78	31.11

	Thermal Maturity Parameters				
sample ID	Ts/Tm	C_{32} 22S/(22S + 22R)	C_{29}20S/(20S + 20R)	$C_{29}\beta\beta/(\beta\beta + \alpha\alpha)$	M_{30}/C_{30}	MPI-1	MPI-2	VRC
TT7	2.67	0.57	0.48	0.51	0.10	0.89	1.09	0.93
TT10	2.83	0.56	0.48	0.56	0.08	0.94	1.18	0.96
TT11	3.00	0.56	0.50	0.55	0.14	0.82	1.03	0.89

[a]Pr—pristane, Ts—(C_{27} 18α (H)-22, 29, 30-trisnorneohopane), CPI—carbon preference index = {2(C_{23} + C_{25} + C_{27} + C_{29})/(C_{22} + 2[C_{24} + C_{26} + C_{28}] + C_{30})}, waxiness degree (WI) = Σ (n-C21- n-C31)/Σ (n-C15- n-C20), Ph—phytane, Tm− (C_{27} 17α (H)-22, 29, 30-trisnorhopane), HCR_{31}/HC_{30}: C_{31} regular homohopane/C_{30} hopane, C_{29}/C_{30}: C_{29} norhopane/C_{30} hopane, G/HC_{30} = gammacerane/C_{30} hopane, M_{30}/C_{30} = C_{30} moretane/C_{30} hopane, DB = dibenzothiophene, Phen = phenanthrene, and MPI-1: methylphenanthrene index = 1.5 × (2 − MP + 3 − MP)/(Phenanthrene + 1 − MP + 9 − MP). MPI-2: methylphenanthrene index = 3 × (2 − MP)/(phenanthrene + 1 − MP + 9 − MP). VRc (%) = 0.60 * MPI-1 + 0.40.

https://doi.org/10.1021/acsomega.3c09003
ACS Omega 2024, 9, 7085−7107

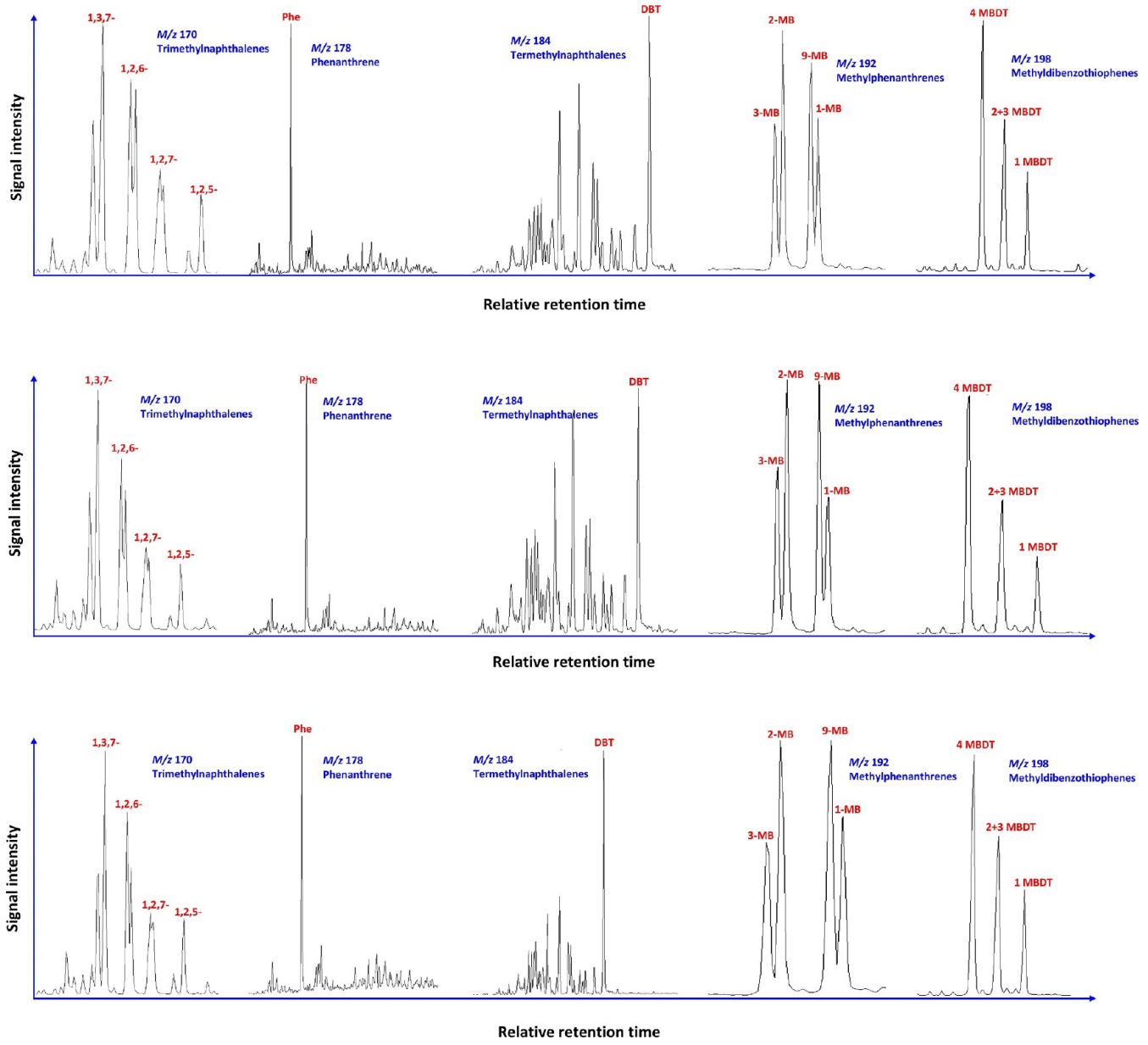

Figure 7. *m*/*z* 170, 178, 184, 192, and 198 mass fragmentograms of the aromatic hydrocarbon fraction in the representative organic-rich shale samples of the Baluti Formation.

such as standard C_{27}/C_{29} regular sterane, C_{29} 20S/(20S + 20R), and $\beta\beta/(\beta\beta + \alpha\alpha)$, as well as C_{27}/C_{29} regular sterane, were further determined (Table 3).

In the current study, polycyclic aromatic compounds such as dibenzothiophene (DBT), phenanthrene (P), alkyl naphthalene, and methylphenanthrene were identified in the aromatic fraction of the investigated three shale samples. These aromatic characteristics and ratios serve as helpful thermometric markers,[56,57] depositional environment and lithologies,[58,59] and source rock facies.[60−62]

The relative distribution of DBF, P, and the homologues of alkyl naphthalene and methylphenanthrene are shown in partial chromatograms of *m*/*z* 184, *m*/*z* 178, *m*/*z* 170, *m*/*z* 192, and *m*/*z* 198, respectively (Figure 7). The relative distribution of these aromatic compounds is used to calculate several aromatic parameters and ratios, such as MDR, MPI-1, MPI-2, and DBT/P, and are presented in Table 3.

4.4. Petrographic and Mineralogical Results. The mineral compositions of the analyzed Baluti shale samples were determined from XRD charts. The results of XRD revealed that the studied Baluti samples comprise an extremely complex mineral composition, including quartz, clay (mainly illite), and pyrite minerals (Figure 8a,b). The distributions of the mineral composition demonstrate that the quartz mineral dominates over the other minerals (Figure 8a,b). The presence of quartz and pyrite minerals, with a high abundance of quartz, was also observed in a thin section under a microscope (Figure 8c−e). The pyrite mineral is represented by an irregular surface, varying shapes, and gray color (Figure 8c,d). However, the enrichment with quartz minerals is considered to be more brittle rocks.[63−65] In this case, the analyzed Baluti shale samples consist of a higher quartz brittle mineral compared to clay mineral (Figure 8a,b). Based on this mineral constituent, the selected Baluti samples are likely to be high-brittle rocks for fracability and the development of natural and artificial fractures.[64,65] Fractures

https://doi.org/10.1021/acsomega.3c09003
ACS Omega 2024, 9, 7085−7107

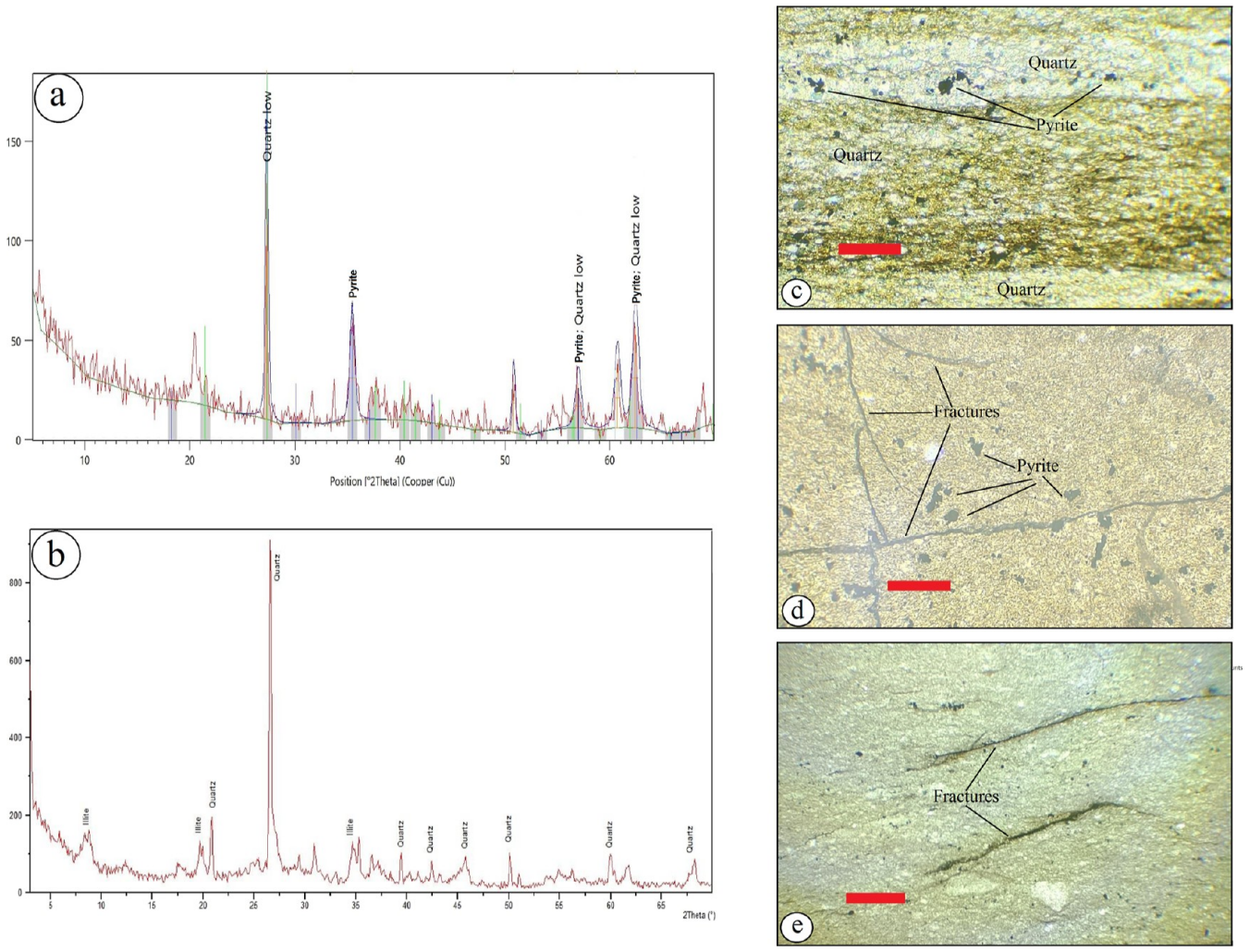

Figure 8. (a,b) X-ray diffractograms of the representative organic-rich shale samples of the Baluti Formation, showing the presence of quartz, illite, and pyrite minerals, and (c−e) photomicrographs of a thin section of the representative organic-rich shale samples of the Baluti Formation, showing the mineral composition and porosity types, including secondary pores such as fracture.

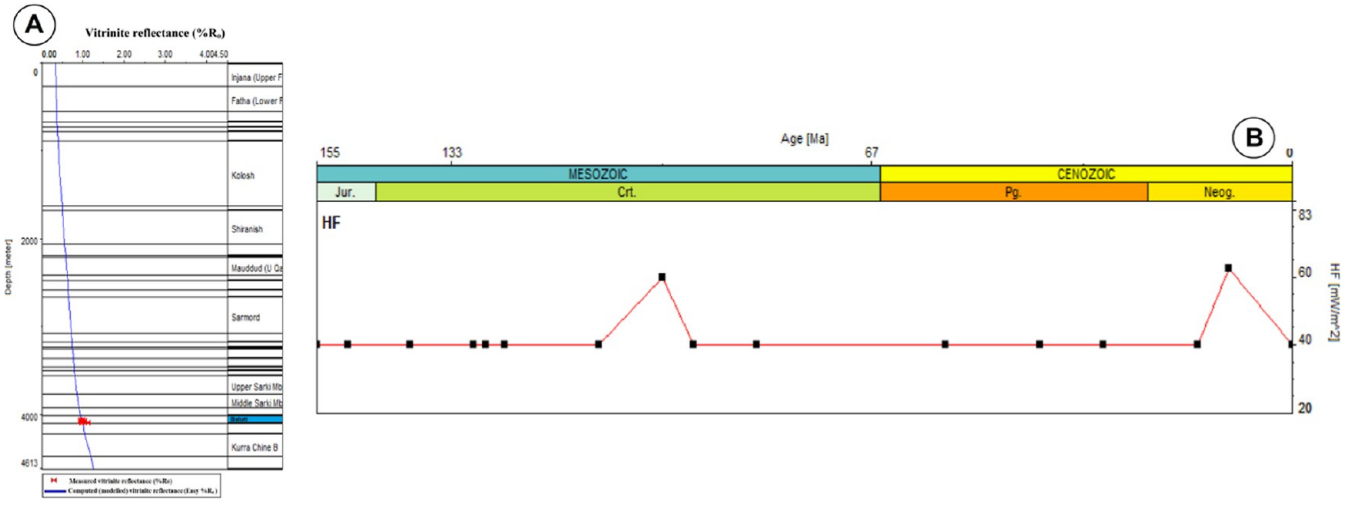

Figure 9. Basin models show (A) an optimized fit of calibrated data, i.e., measured % VRo and models of EASY % Ro maturity in the studied well (TT-22), and (B) the estimated HF range that achieved from calibration data (% VRo).

seen in the examined shale samples provided support for this interpretation (Figure 8d,e).

4.5. Basinal Thermal Evolution and Maturation of Source Rock. The period of source rock maturation is influenced by thermal geo-history development in sedimentary

https://doi.org/10.1021/acsomega.3c09003
ACS Omega 2024, 9, 7085−7107

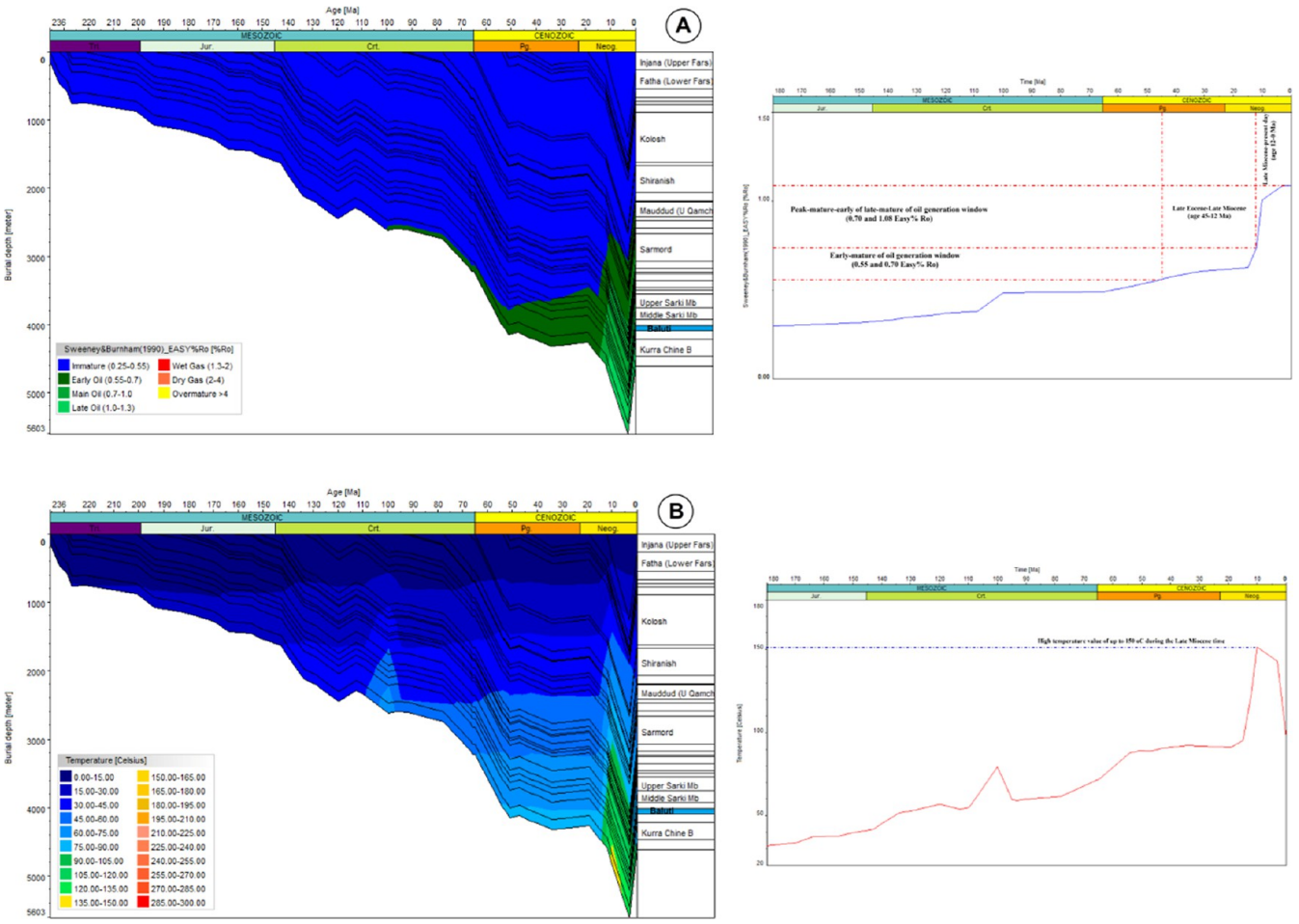

Figure 10. (A) Burial overlap with thermal maturity (colored areas) cross all rock units (left) and the blue line are shown exclusively for computed VRo (right), and (B) burial overlap with thermal gradient history (colored areas) cross all rock units (left) and the red line are shown exclusively for computed temperatures (right) of the base Baluti Formation in the studied TT-22 well.

basins, which affects petroleum generation over the course of geological time.[42,66] The key elements that influence a basin's thermal history include sedimentation, erosion history, burial temperature slopes, temperature gradients, and paleo-HFs.[67]

Using a 1-D-basin simulation method, the measured % VRo (available from the exploratory well; Table 1) was used to determine the paleo-HF values. Here, several HF model scenarios are used in conjunction with erosion episodes that occurred in the late Pliocene (3 Ma; Table 2). By including the erosional history, a passable fit of Sweeney and Burnham's[52] maturation (Easy % Ro) and measured VRo profiles is obtained (Figure 9a). In order to achieve the best fit between measured % VRo and modeled EASY % Ro, elevated HF values between 40 and 68 mW/m^2 were assigned (Figure 9b). However, Allen and Allen[42] indicated that the paleo-HF values between 40 and 80 mW/m^2 are considered for foreland basins. The HF model employed in this study reveals that paleo-HF values during the Late Cretaceous and Miocene periods were relatively high, ranging between 60 and 68 mW/m^2 (Figure 9b). This is related to the Zagros Mountains' development as a result of the Arabian and Iranian plates' reactive convergence and collision during the Mid-Late Cretaceous (Zagros Orogeny) and the foreland basin of the ZFB in northern Iraq.[68−73]

However, we employed modeled HF to reconstruct the thermal maturation history of the Late Triassic Baluti Formation and pinpoint the time of petroleum formation (Figure 9). According to the maturity models, the Baluti Formation is currently in the peak-to-late-mature of the oil generation window (Figure 10a). These models further show that the thermal gradient has a significant impact on the thermal maturation history of the studied Baluti shales and that the base of the Baluti Formation extends down to a depth of more than 4000 m, resulting in high burial temperatures of around 157 °C during the Late Miocene (Figure 10b). Following that, the Baluti Formation's base enters the early mature oil window (0.55−0.70 Easy % Ro) during the Late Eocene to Late Miocene time (45−12 Ma; Figure 10a). Peak oil production occurred during the Late Miocene (12 Ma) and has continued until today. This corresponds to an Easy % Ro value between 0.70 and 1.08 (Figure 10a) and a temperature value of up to 150 °C (Figure 10b).

5. DISCUSSION

5.1. Source of OM and Paleoenvironmental Conditions. The intake of OM, its origin, and the depositional environment of the Baluti shales were assessed based on accepted standard interpretations of molecular biomarker proxies in light of the saturated and aromatic biomarker data.[74−77] The unimodal distribution of normal alkanes in GC may signify a significant contribution from marine OM made up of algae microbial mats, which is dominated by n-C_{13} to n-C_{26} molecules of short to medium molecular weight (Figure 5). The

https://doi.org/10.1021/acsomega.3c09003
ACS Omega 2024, 9, 7085−7107

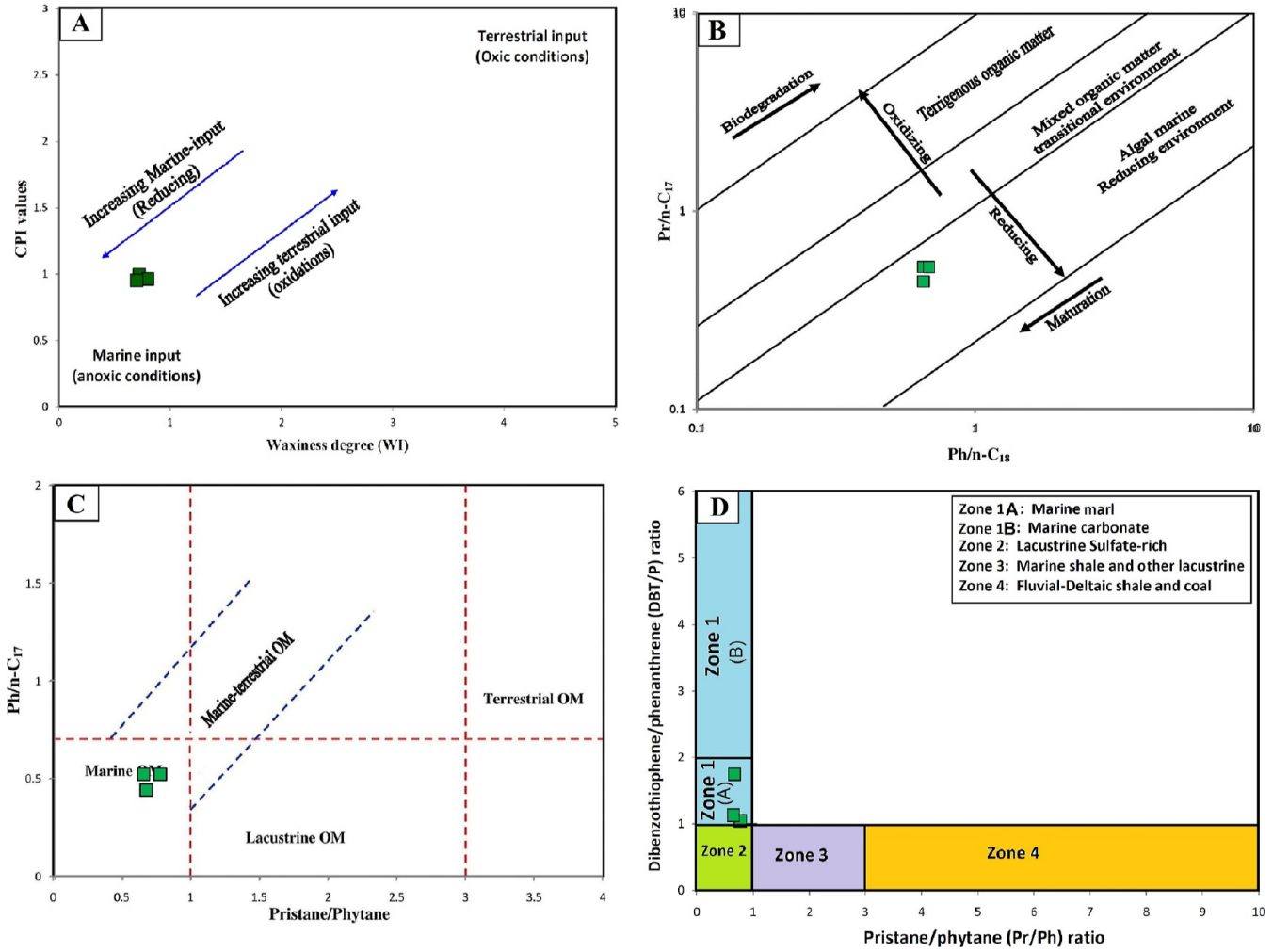

Figure 11. Geochemical biomarker results of the representative three shale samples of the Baluti Formation from TT-22 well, including (A) CPI and WI degree, (B) Pr/*n*-C_{17} versus Ph/*n*-C_{18}, (C) Pr/Ph versus Pr/*n*-C_{17}, and (D) Pr/Ph versus DPT/P ratio, indicate that the Baluti shale sediments contain mainly marine OM and were deposited under anoxic conditions.

contribution of the different OM inputs may also be deduced using CPI and WI degree values.[78,79] Lower CPI and WI values reveal a higher contribution of aquatic OM.[74] In this case, the combination of CPI and further support the increased contributions from marine OM and some terrestrial source input into these shale strata (Figure 11a).

The OM present in the redox depositional environment was also assessed from the isoprenoids.[80,81] In this case, the relatively high concentrations of Ph (Figure 5), with low Pr/Ph, Pr/*n*-C_{17}, and Ph/*n*-C_{18} ratios, further point to algal marine-derived OM and highly reductive conditions during deposition (Figure 11b,c). The depositional conditions may also be deduced using the Pr/Ph isoprenoid ratio.[80] Pr/Ph < 1 denotes an anoxic environment with a stratified water column, while Pr/Ph > 2 denotes contributions from terrestrial OM under oxic environmental conditions, according to Didyk et al.,[80] and Chandra et al.[81] Most of the shale samples show low Pr/Ph values ranging from 0.65 to 0.77 (Table 3), indicating that these shales were accumulated during anoxic depositional settings.

In addition, the combination of the Pr/Ph ratio together with the high DBT/Phen ratios of >1 supports the interpretation of a marine source rock (Figure 11d). The distribution of the C_{31} homohopanes in the *m*/*z* 191 mass fragmentograms lends credence to this interpretation.[71] The C_{30} hopane dominates in comparison to the C_{31}R homohopane (Figure 6b), and the ratio of $C_{31}R/C_{30}$ is relatively high, ranging from 0.24 to 0.30 (Table 3), suggesting that the Baluti rocks were formed in a marine environment.

The occurrence of a significant concentration of tricyclic terpanes in the *m*/*z* 191 mass fragmentograms (Figure 6a), with the ratios of C_{26}/C_{25}, C_{22}/C_{21}, and C_{24}/C_{23} tricyclic terpanes (Table 3) also suggests this understanding for a high contribution of marine OM into the Baluti source rocks (Figure 12).

Using the modified ternary diagram from Huang and Meinschein[82] (Figure 13), the high concentrations of C_{27} regular sterane in all of the examined shale samples (Table 3) support the interpretation of primarily planktonic and bacterial origin, with little input of OM derived from plants. Additionally, the existence of high C_{27}/C_{28} regular sterane ratios supports this (Table 3).

Organic material from aquatic sources contributed significantly to the Baluti shales in a relatively oxygen-poor environmental setting, as confirmed by the relatively low proportions of 1,2,5- and 1,2,7-trimethylnaphthalene compared to 1,3,7- and 1,2,6-trimethylnaphthalene in the aromatic fraction (Figure 7). According to Strachan et al.,[83] the relative abundance of 1,2,5- and 1,2,7-trimethylnaphthalene is likely to indicate a

https://doi.org/10.1021/acsomega.3c09003
ACS Omega 2024, 9, 7085−7107

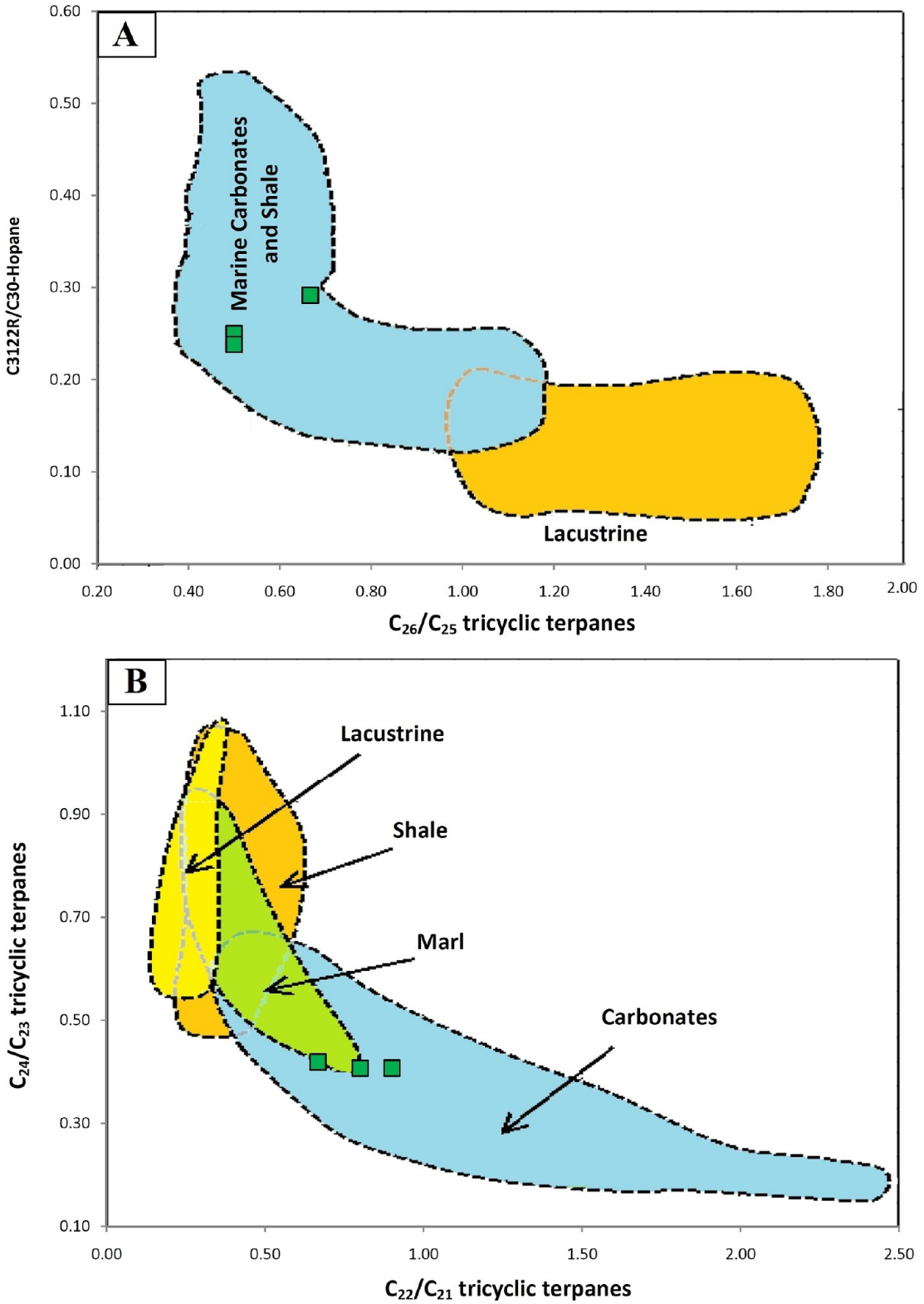

Figure 12. Geochemical biomarker results of the analyzed organic-rich shale samples show (A) C_{26} tricyclic/C_{25} tricyclic ($C_{26}T/C_{25}T$) versus C_{31} regular homohopane/C_{30}hopane (HCR_{31}/HC_{30}) and (B) C_{24} tricyclic/C_{23} tricyclic ($C_{24}T/_{23}T$) versus C_{22} tricyclic/C_{21} tricyclic ($C_{22}Ti/C_{21}Ti$), indicating that these sediments contain mainly marine OM.

larger supply of plant OM and a deltaic environment with relatively high oxygen levels.[84]

5.2. Characterization and Efficiency of the Source Rock for the Potential of Hydrocarbon Generation. Most of the Baluti shales are organic-rich, with a high TOC content of more than 1 wt % and reaching maximum TOC % of 4.92 wt % (Table 1). Considering that most organic geochemists reported that sediments with a TOC level of more than 1% suggest a sufficient amount of OM for a good source rock.[85,86] Therefore, the high TOC content of more than 1 wt % in most of the Baluti

https://doi.org/10.1021/acsomega.3c09003
ACS Omega 2024, 9, 7085−7107

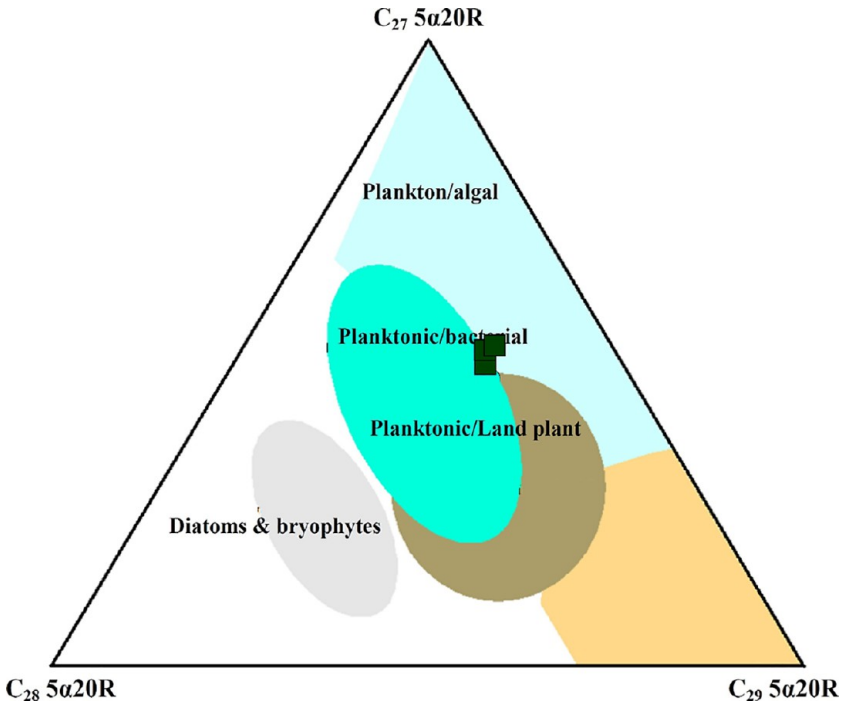

Figure 13. Ternary diagram of regular steranes (C_{27}−C_{29}) in the saturated HC fraction of the representative three shale samples of the Baluti Formation from TT-22 well, indicating the relationship between sterane compositions concerning OM input.

shales indicates good source rock characteristics for noteworthy amounts of petroleum-generating potential at thermal maturation. This finding is confirmed by the relationship between TOC and the petroleum yield obtained by thermal cracking of kerogen (S_2). The TOC results correlate well with the petroleum potential yield (S_2) and further reveal a good to very good generative potential for most of the examined Baluti samples (Figure 14a).

The high TOC content in the studied Baluti samples was further combined with the pyrolysis S_1 petroleum yield and used to calculate the oil saturation index (OSI mg/gram) using the following formula: OSI = $S_1 \times 100/\text{TOC}$.[61,87,88] The capacity of the oil-bearing source rock and the potential economically producible oil were also estimated using this ratio.[64,87,88] A mature source rock is represented by OSI values more than 30, whereas an oil-saturated source rock is indicated by values between 50 and 70.[87] Likewise, oil crossover is defined as the OSI ratio above 100%, which demonstrates the source rock's capacity to hold oil.[87,88]

In this study, the 13 shale samples from the Baluti Formation have OSI values ranging from 125.93 to 448.98 mg/g and are shown in Table 1. The majority of the analyzed samples from the studied well with OSI values of >100 mg/g represent the oil crossover effect and may serve as a significant benchmark for significant quantities of oil-bearing material and increase the likelihood of oil production (Figure 14b).

The present study also integrates bulk RE data and microscopic examination results to understand kerogen's characteristics and classification within the investigated Baluti shale samples.

The RE parameters HI and OI were employed to evaluate the qualitative kerogen classification using the OI vs HI diagram. In this diagram, the majority of the shale samples under examination fell along the hydrogen-rich type I and II kerogen paths, with just a modest contribution from types II/III and III kerogen (Figure 15a). The domination of hydrogen-rich type I and II kerogens was also reinforced by the relationship between the HI and T_{max} (Figure 15b). Therefore, based on the kerogen, it is expected that the Baluti shales can generate high amounts of oil as implied by the relationship between the TOC content and the pyrolysis HI parameter (Figure 16).

The thermal alteration of OM in the studied shale unit of the Baluti Formation from the selected well was assessed using multiple optical and geochemical indicators (Tables 1 and 3). The results of this integration enable us to assess the thermal maturity level of OM input and its potential for petroleum generation.

VRo % data are among the most reliable parameters to highlight maturity and focus on critical information, such as the degree of maturation of organic material and the ability to generate petroleum.[45]

Seven shale samples from the Baluti Formation taken from the TT-22 well were used in the current investigation to evaluate the thermal changes of OM. In Table 1, the measured VR values for the Baluti shale samples are shown. This range, which represents the peak-mature to late-mature of the oil-generating window, is between 0.92 and 1.15%.

The T_{max} values were also used to assume organic maturity. The T_{max} data of the analyzed samples varies between 301 and 435 °C (Table 1), indicating immature to early mature oil window. These stages of thermal maturity from T_{max} are inconsistent with the VRo %-based observation. We envisage that the presence of generated hydrocarbons within the studied shales might have lowered T_{max} values (<430 °C) at deeper burial depths.[89] The presence of generated hydrocarbons in the samples is confirmed by the relatively higher S_1 as compared to TOC content (Table 1), and hence, high PI values of more than 0.40 (Figure 17). Therefore, the RE T_{max} values of <430 °C were not trustworthy thermal maturation indicators in the deeper Baluti shale samples.

https://doi.org/10.1021/acsomega.3c09003
ACS Omega 2024, 9, 7085−7107

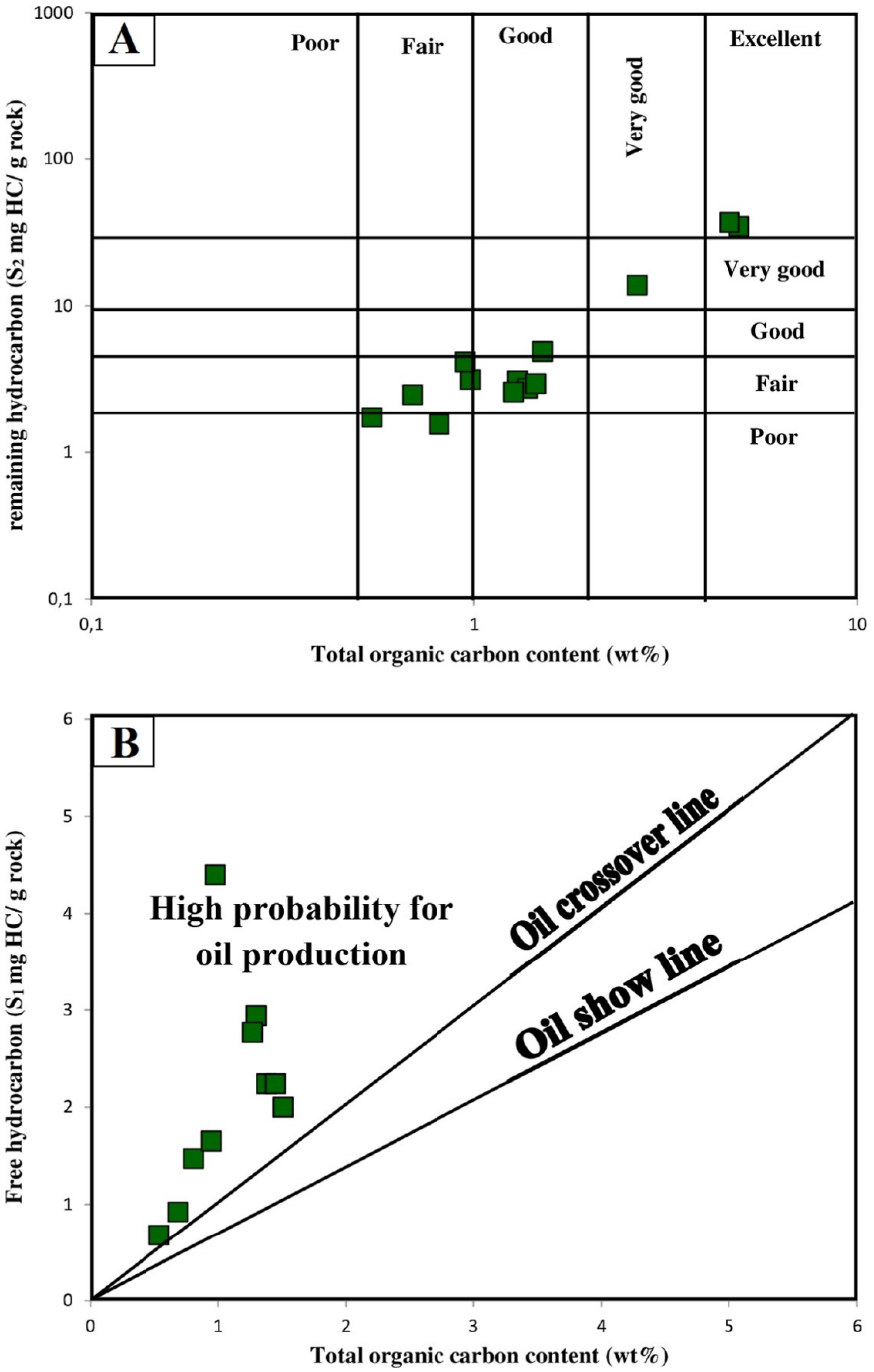

Figure 14. Geochemical correlations between TOC content and RE pyrolysis parameters [i.e., S_2 and S_1 in (A,B), respectively] imply that the analyzed organic-rich shales from the studied well are considered to be good source rocks and have a high probability of oil production.

Herein, the source rock maturity of the Baluti formation was also concluded from specific maturity-derived biomarkers based on established standard classifications. These maturity-derived biomarkers most commonly used to establish maturity include those derived from terpane, sterane, and methylphenanthrene content of the hydrocarbon fractions, i.e., aliphatic and aromatics,[51,52,90−93] including Ts/Tm, C_{32} hopane, 20S/(20S + 20R), and $\beta\beta/(\beta\beta + \alpha\alpha)$ of C_{29} sterane and methylphenanthrene indices (i.e., MPI-1 and MPI-2) (Table 3).

The hopane ratio of C_{32} 20S/(20S + 20R) can range up to values of 0.7, reflecting high maturity, although it is most reliable at lower maturities.[92] When paired with high C_{29} sterane $\beta\beta/(\beta\beta + \alpha\alpha)$ ratios, almost all of the studied samples exhibit reasonably high C_{32} hopane ratios of 0.56 to 0.57, indicating that the Baluti source rock has matured to its peak oil window (Figure 18a). Further, the C_{29} sterane ratios of the $\beta\beta/(\beta\beta + \alpha\alpha)$ and 20S/(20S + 20R) may also suggest the analyzed Baluti shale samples are mature source rocks (Figure 18b).

The high maturity source rock of the examined samples is also suggested by the high trisnorneohopane (Ts) in m/z 191 MC (Figure 6a), with high Ts/Tm ratios greater than 2 (Table 3). The high Ts/Tm index is consistent with the low ratio of C_{30} moretane/C_{30} hopane (CM_{30}/C_{30}) and further suggests mature source rock of the peak oil window (Figure 18c). However, these

https://doi.org/10.1021/acsomega.3c09003
ACS Omega 2024, 9, 7085−7107

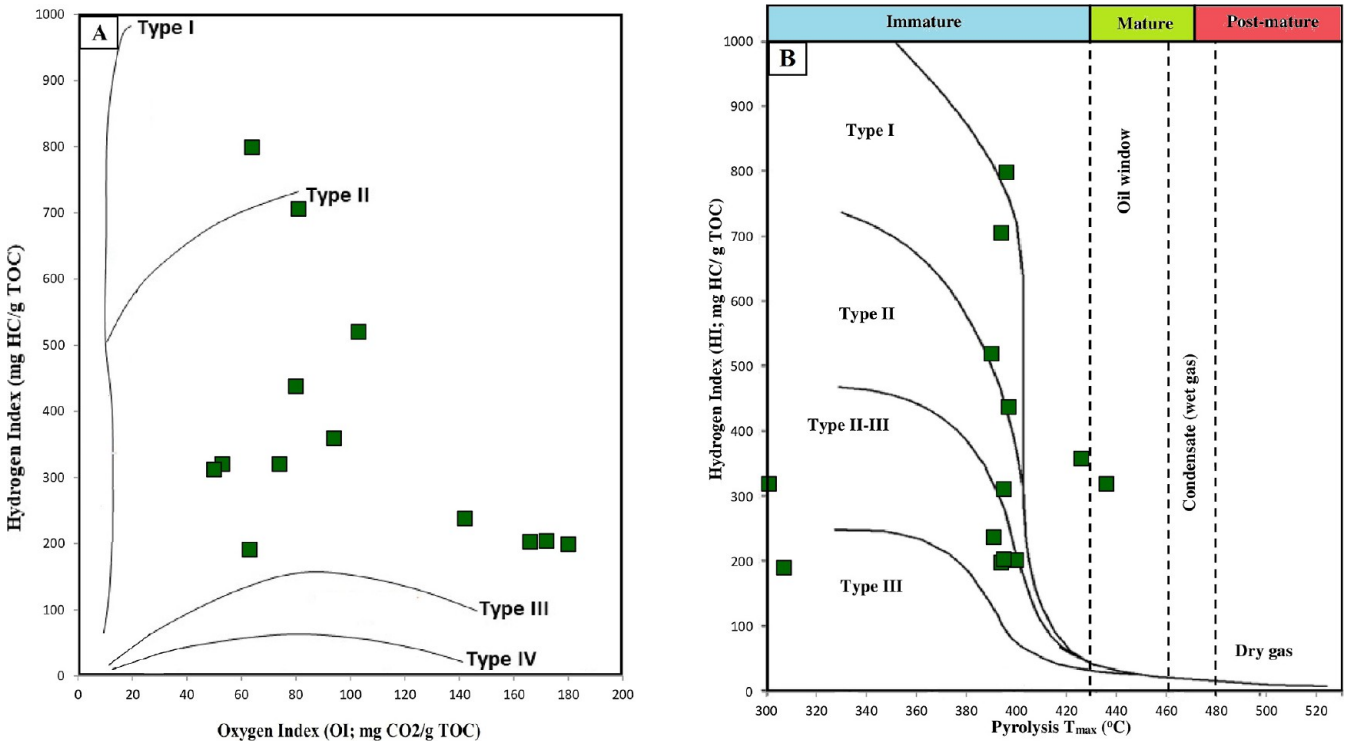

Figure 15. Characteristics of kerogen of the organic-rich shale samples of the Baluti Formation from the studied TT-22 well based on (A) HI versus OI and (B) HI versus T_{max}, showing hydrogen-rich types I and II and small amounts of types II/III and III kerogens.

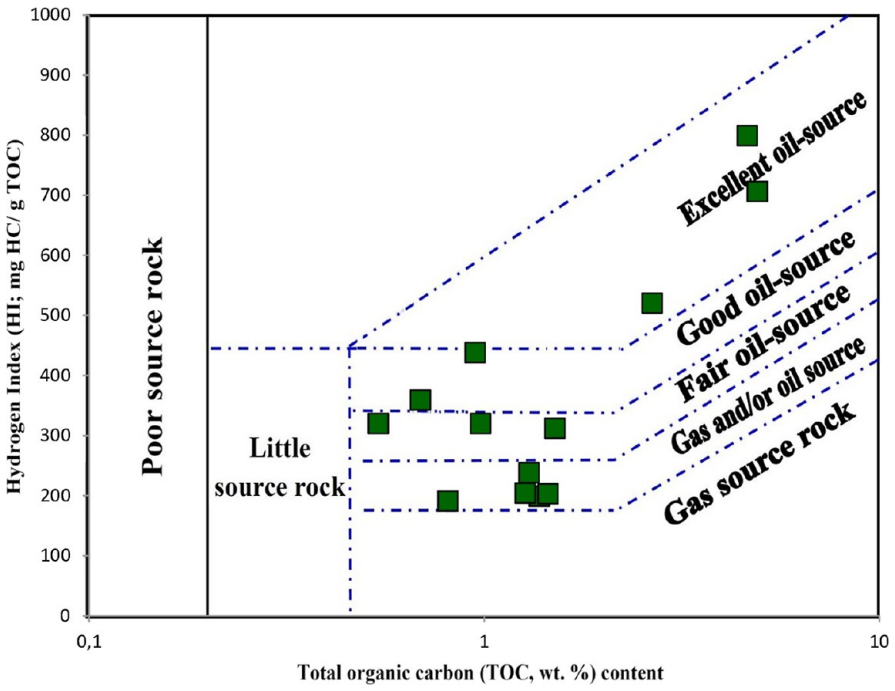

Figure 16. Geochemical correlation between TOC content and RE data (i.e., HI), implying that the analyzed organic-rich shales samples of the Baluti Formation from the studied TT-22 well are mainly oil-prone source rocks.

hopane and sterane maturity biomarkers alone are therefore not sufficient to evaluate thermal maturity and must be matched with other maturity-sensitive aromatic biomarkers.

With increasing age, the relative abundance of more stable isomers rises in comparison to less stable isomers because the aromatic maturity characteristics are often based on the variable thermal stability of distinct isomers.[56] The MPI-1 and MPI-2 indices of phenanthrene are among the computed aromatic parameters for the samples that were analyzed (Table 3). The high MPI-1 and MPI-2 values in the studied shale samples (ranges of 0.82−0.94 and 1.03−1.18, respectively) point to a mature source rock (Table 3 and Figure 18d). The VRo values from MPI-1 were also calculated, ranging from 0.89 to 0.96% (Table 3), consistent with a peak-mature oil window.

https://doi.org/10.1021/acsomega.3c09003
ACS Omega 2024, 9, 7085−7107

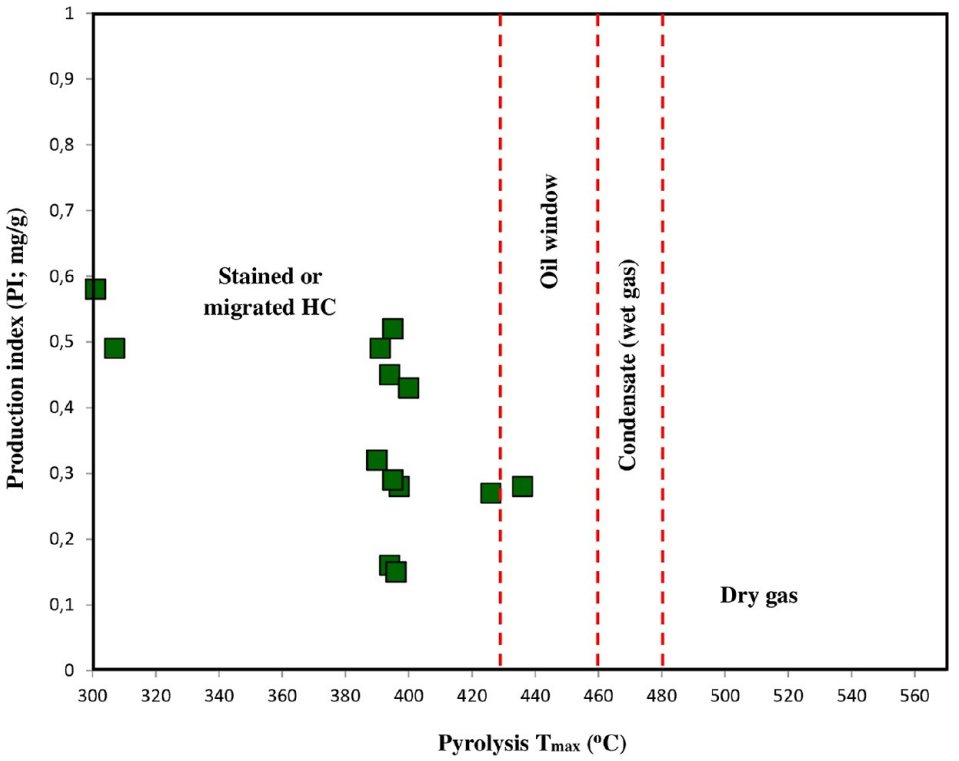

Figure 17. Thermal maturity indicators (i.e., T_{max} and PI) of the organic-rich shale samples of the Baluti Formation, including analyzed samples in the studied TT-22 well mainly containing staining or migrated HCs.

5.3. Implications for Oil Exploration Opportunities. In the studied TT-22 well from Taq Taq oilfield, the Baluti organic-rich shales have a high abundance of main types I and II kerogen and are currently in the high maturity stage of the oil window (i.e., peak-mature to late-mature), implying that commercial quantities of oil have been generated. On the other hand, the high OSI values of more than 100 mg/g confirm that the Baluti source rock system has generated a considerable quantity of oil and is saturated now, leading to a high probability for oil production (Figure 14b). The higher amount of oil accumulation in the Baluti source rock system from the TT-22 well is also confirmed through basin model results.

Modeling of the primary kerogen cracking and oil production from the Baluti source rocks across geological time (Figure 19). These conversion ratio models were developed using the type I kinetic data of Behar et al.[94] Based on the type I kinetic reaction parameters, thermal maturity, and burial history, the primary kerogen-oil cracking and retained oil cracking to the gaseous phase from type I source rock were timed.

The TT-22 well-based model suggests that the Baluti source rock reached a TR of 10−50% (Figure 19a) and had generated substantial volumes of oil during the late Miocene age around 12 to 7 Ma (Figure 19b), corresponding to computed VR values in the ranges of 0.77−1.02% (Figure 10a). From the end of the late Miocene (7 Ma) to the present, tiny amounts of oil produced in the Baluti source rock system have been released, with TR values exceeding 50% (Figure 19a). However, the Baluti source rock has generated its maximum amount of oil and is saturated, suggesting that the greatest values are more than 50% for its kerogen conversion, which led to high pressures and pushed the brittle minerals to be shattered, resulting in a natural fracture system (Figure 8c,d). This natural fracture system can develop the porosity of the tight shale rocks of the Baluti Formation, resulting in better potential oil storage capability. As a result, the fracability of the Baluti shale rocks is identical for hydraulic stimulation, making them ideal for oil production.[64,88] Meanwhile, the oil bearing of the shale for oil production is associated with oil generation and expulsion.[88] Shales with higher oil generation and lower oil expulsion features are ideal for shale oil resource discoveries.[88] The Baluti organic-rich shales attained TR values between 10 and 65%, as indicated in the basin modeling results (Figure 19a). Therefore, the Baluti source rock system should have a lower oil expulsion efficiency (TR up to 65%) and thus higher residual oil as well as oil-bearing capacity, making it a suitable prospect for shale oil discoveries. This significant find will help shale oil prospects and exploration targets in the northern Iraqi basin of the ZFB, where the Late Triassic Baluti Formation candidates as unconventional petroleum resources, and it will lead to the production of more oil that could be released using hydraulic fracturing techniques.

6. CONCLUSIONS

This study investigated the Late Triassic Baluti Formation's organic-rich shale and potential oil production in northern Iraq's ZFB. The present investigation provides the following findings:

- The Late Triassic Baluti Formation, which has a TOC of approximately 4.92 wt % and primarily types I and II kerogens with a trace amount of types II/III and III, is a notable oil-source rock.
- The OM origin and depositional environment-related biomarkers suggest that the OM input to the Baluti shale source rock is a mixture of mainly phytoplankton and bacteria with a small amount of terrigenous plants and deposited under marine reducing conditions.
- A number of maturity-related indicators show that the investigated samples of the Baluti Formation have

https://doi.org/10.1021/acsomega.3c09003
ACS Omega 2024, 9, 7085−7107

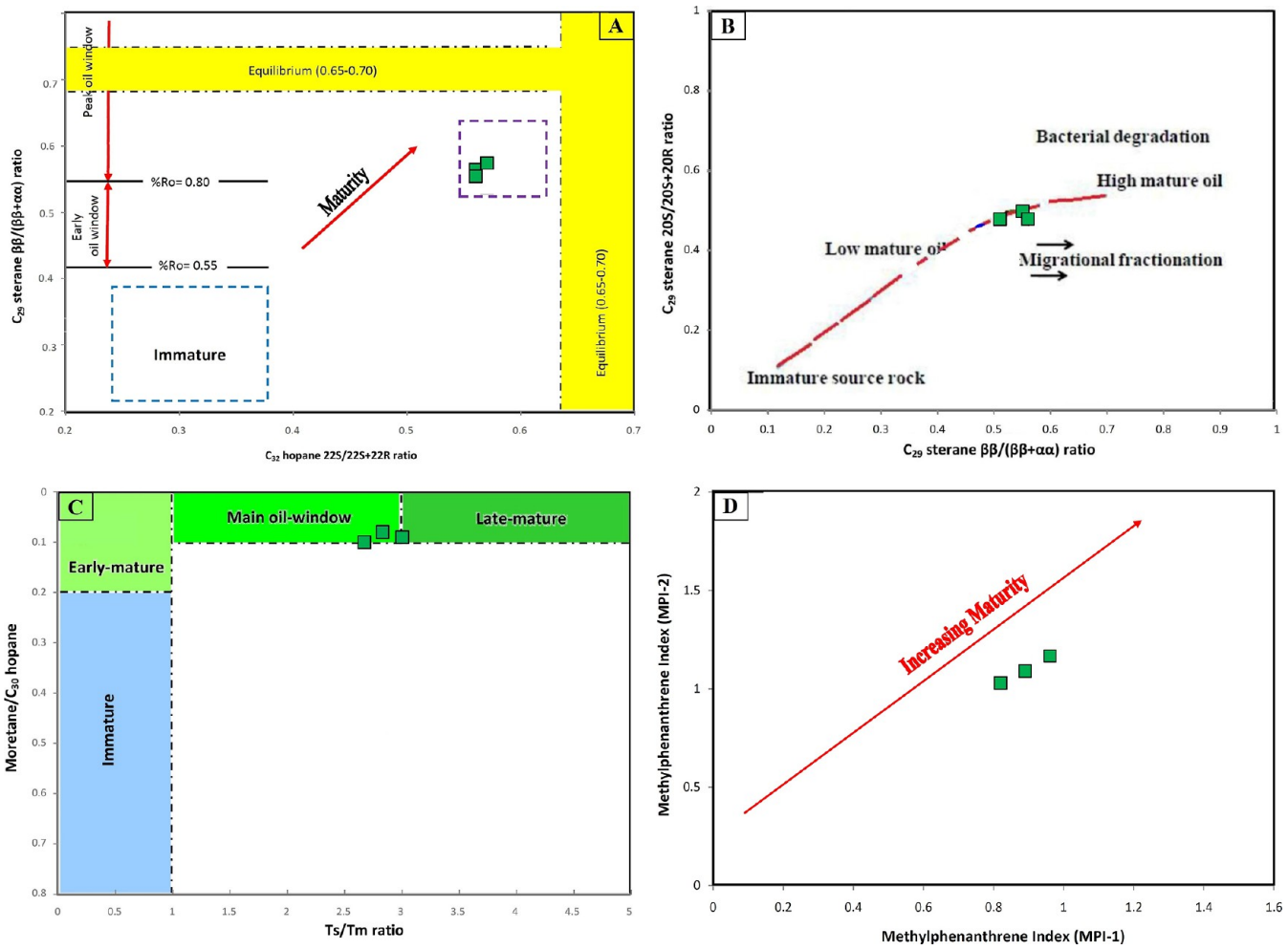

Figure 18. Geochemical cross-plot of the biomarker maturity indicators of the analyzed shale samples (A) C_{32}-hopane 22 S/(22S + 22R) versus C_{29} sterane $\beta\beta/(\beta\beta + \alpha\alpha)$, (B) C_{29}-sterane 20 S/(20S + 20 R) versus $\beta\beta/(\beta\beta + \alpha\alpha)$, (C) M_{30}/C_{30} versus Ts/Tm ratio, and (D) MPI-1 versus MPI-2 ratio, showing the high thermal maturation of the Baluti shale samples, corresponding to main stage of petroleum generation (i.e., peak oil generation window).

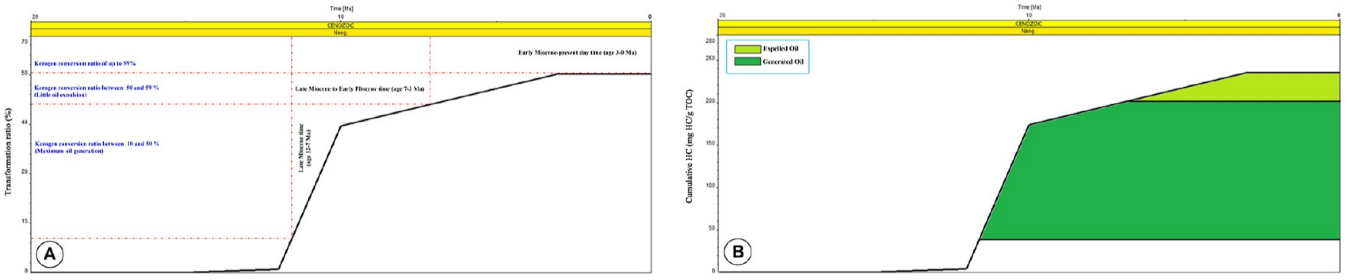

Figure 19. (A) Evolution of the TR and computed VRo (EASY % Ro) with age and (B) model of cumulative hydrocarbon generation for the base Baluti Formation in the studied TT-22 well.

attained a variety of thermal maturation stages, from peak-mature to late-mature oil windows.

- The majority of the Baluti Formation's organic-rich shales crossed the oil-crossover, indicating good oil-bearing capacity and enrichment conditions for high-probability oil production matched with OSI values above 100 mg/g.
- The basin model study, enriched with geological data, has revealed a primary kerogen-oil conversion of the Baluti source rock occurred between the late Miocene and the present (12−0 Ma), with the main oil window maturity (0.77−1.08 Easy % Ro) and 10−59 % TR.
- When the maximum TR (59% TR) was attained at the end of the late Miocene, a small amount of oil was released from the Baluti source rock system.
- The natural fracture system in the Baluti shale source rock was recognized and observed in thin sections. This natural fracture system is probably attributed to the combination between the high quartz brittle mineral content and the presence of significant amounts of oil generation with lower oil expulsion efficiency.
- The above characteristics of the Baluti shale source rock system can be used as a foundation for further shale oil

https://doi.org/10.1021/acsomega.3c09003
ACS Omega 2024, 9, 7085−7107

exploration in the Taq Taq oilfield, where the Baluti Formation serves as a candidate for source-self-reservoir potential and could result in high-probability oil production that could be released using hydraulic fracturing techniques.

AUTHOR INFORMATION

Corresponding Author

Mohammed Hail Hakimi − *Department of Geology, Faculty of Applied Science, Taiz University, Taiz 6803, Yemen;* orcid.org/0000-0002-3320-9690; Email: ibnalhakimi@yahoo.com

Authors

Ibrahim M. J. Mohialdeen − *Department of Geology, University of Sulaimani, Sulaimani 46001 Kurdistan Regional Government, Iraq;* orcid.org/0000-0003-4544-3959

Sardar S. Fatah − *Department of Geology, University of Sulaimani, Sulaimani 46001 Kurdistan Regional Government, Iraq*

Rzger A. Abdula − *Department of Petroleum Geosciences, Soran University, Kurdistan 44008, Iraq; Petroleum and Mining Engineering Department, Tishk International University, Erbil 44001 Kurdistan, Iraq*

Polla A. Khanaqa − *Kurdistan Institute for Strategic Studies and Scientific Research, Sulaimani 46001 Kurdistan, Iraq*

Mahdi Ali Lathbl − *Department of Geoscience, Universiti Teknologi PETRONAS, Seri Iskandar 32610 Perak, Malaysia*

Waqas Naseem − *Department of Geology, University of Poonch Rawalakot, Azad Jammu& Kashmir Rawalakot 12350, Pakistan*

Complete contact information is available at: https://pubs.acs.org/10.1021/acsomega.3c09003

Notes

The authors declare no competing financial interest.

ACKNOWLEDGMENTS

The authors gladly thank the financial support for the project from the Ministry of Higher Education and Scientific Research of the Kurdistan Regional Government (grant no. 10238/1 of 8/8/2018). It is also greatly appreciated that the Kurdistan Regional Government's Ministry of Natural Resources assisted in facilitating access to samples used in this study. We would like to thank Mr. Grenville Lunn for helping in drawing Figure 4. Two anonymous reviewers are thanked for the constructive comments that improved the original manuscript.

REFERENCES

(1) Sohail, G. M.; Radwan, A. E.; Mahmoud, M. A review of Pakistani shales for shale gas exploration and comparison to North American shale plays. *Energy Rep.* **2022**, *8*, 6423−6442.

(2) Hill, R. J.; Zhang, E.; Katz, B. J.; Tang, Y. Modeling of gas generation from the Barnett shale, Fort Worth Basin, Texas. *Am. Assoc. Petrol. Geol. Bull.* **2007**, *91* (4), 501−521.

(3) Nie, H.; Jin, Z.; Li, P.; Jay Katz, B.; Dang, W.; Liu, Q.; Ding, J.; Jiang, S.; Li, D. Deep shale gas in the Ordovician-Silurian Wufeng−Longmaxi formations of the Sichuan Basin, SW China: Insights from reservoir characteristics, preservation conditions and development strategies. *J. Asian Earth Sci.* **2023**, *244*, 105521.

(4) Qadri, S. M. T.; Islam, M. A.; Shalaby, M. R.; Ali, S. H. Integration of 1D and 3D modeling schemes to establish the Farewell Formation as a self-sourced reservoir in Kupe Field, Taranaki Basin, New Zealand. *Front. Earth Sci.* **2021**, *15*, 631−648.

(5) Radwan, A. E.; Wood, D. A.; Mahmoud, M.; Tariq, Z. Gas adsorption and reserve estimation for conventional and unconventional gas resources. *Sustainable Geoscience for Natural Gas Subsurface Systems*; Gulf Professional Publishing, 2022; pp 345−382.

(6) Al-Ahmed, A. A. Organic Geochemistry, Palynofacies and Hydrocarbon Potential of Sargelu Formation (Middle Jurassic) Northern Iraq. Ph.D. Thesis, University of Baghdad (Unpublished), 2006.

(7) Al-Ameri, T. K.; Zumberge, J. Middle and upper Jurassic hydrocarbon potential of the Zagross Fold Belt, North Iraq. *Mar. Petrol. Geol.* **2012**, *36*, 13−34.

(8) Hakimi, M. H.; Najaf, A. A. Origin of crude oils from oilfields in the Zagros Fold Belt, southern Iraq: Relation to organic matter input and paleoenvironmental conditions. *Mar. Petrol. Geol.* **2016**, *78*, 547−561.

(9) Mohialdeen, I. M. J.; Hakimi, M. H. Geochemical characterisation of Tithonian-Berriasian Chia Gara organic-rich rocks in northern Iraq with an emphasis on organic matter enrichment and the relationship to the bioproductivity and anoxia conditions. *J. Asian Earth Sci.* **2016**, *116*, 181−197.

(10) Mohialdeen, I. M. J.; Hakimi, M. H.; Al-Beyati, F. M. Geochemical and petrographic characterization of late Jurassic-early Cretaceous Chia Gara Formation in Northern Iraq: palaeoenvironment and oil-generation potential. *Mar. Petrol. Geol.* **2013**, *43*, 166−177.

(11) Mohialdeen, I. M. J.; Hakimi, M. H.; Al-Beyati, F. M. Biomarker characteristics of certain crude oils and the oil-source rock correlation for the Kurdistan oilfields, Northern Iraq. *Arabian J. Geosci.* **2015**, *8*, 507−523.

(12) Sachsenhofer, R. F.; Bechtel, A.; Gratzer, R.; Rainer, T. M. Source-rock maturity, hydrocarbon potential and oil-source rock correlation in well Shorish-1, Erbil province, Kurdistan Region, Iraq. *J. Petrol. Geol.* **2015**, *38*, 357−381.

(13) Hakimi, M. H.; Najaf, A. A.; Abdula, R. A.; Mohialdeen, I. M. J. Generation and expulsion history of oil-source rock (Middle Jurassic Sargelu Formation) in the Kurdistan of north Iraq, Zagros folded belt: Implications from 1D basin modeling study. *J. Pet. Sci. Eng.* **2018**, *162*, 852−872.

(14) Gharib, A. F.; Özkan, A. M.; Hakimi, M. H.; Zainal Abidin, N. S.; Lashin, A. A. Integrated geochemical characterization and geological modeling of organic matter-rich limestones and oils from Ajeel Oilfield in Mesopotamian Basin, Northern Iraq. *Mar. Pet. Geol.* **2021**, *126*, 104930.

(15) Al-Ameri, T. K.; Najaf, A. A.; Al-Khafaji, A. S.; Zumberge, J.; Pitman, J. Hydrocarbon potential of the Sargelu formation, North Iraq. *Arabian J. Geosci.* **2014**, *7*, 987−1000.

(16) Mohialdeen, I. M. J. Source Rock Appraisal and Oil-source Correlation for the Chia Gara Formation, Kurdistan-north Iraq. Ph.D. Thesis, College of Science, University of Sulaimani, 2008, pp 15−35.

(17) Talbot, C. J.; Alavi, M. *The Past of a Future Syntaxis across the Zagros 100*; Geological Society: London, Special Publications, 1996; pp 89−109.

(18) Koshnaw, R. I.; Horton, B. K.; Stockli, D. F.; Barber, D. E.; Tamar-Agha, M. Y.; Kendall, J. J. Neogene shortening and exhumation of the Zagros fold-thrust belt and foreland basin in the Kurdistan region of northern Iraq. *Tectonophysics* **2017**, *694*, 332−355. Elsevier B.V.

(19) Tozer, R. S. J.; Hertle, M.; Petersen, H. I.; Zinck-Jorgensen, K. Quantifying vertical movements in fold and thrust belts: subsidence, uplift and erosion in Kurdistan, northern Iraq. In *Fold and Thrust Belts: Structural Style, Evolution and Exploration*; Hammerstein, J. A., Dcuia, R., Cottam, M. A., Zamora, G., Butler, R. W. H., Eds.; Geological Society, London, Special Publications, 2019; Vol. *490*, pp 397−415.

(20) Rashid, F.; Hussein, D. H.; Lawrence, J. A.; Khanaqa, P. Characterization and impact on reservoir quality of fractures in the cretaceous Qamchuqa Formation, Zagros folded belt. *Mar. Petrol. Geol.* **2020**, *113*, 104117.

(21) (a) Al-Sharhan, A. S.; Nairn, A. E. *Sedimentary Basins and Petroleum Geology of the Middle East*; Elsevier Science, 2003. (b) Aqrawi, A. A.; Goff, J. C.; Horbury, A. D.; Sadooni, F. N. *The Petroleum Geology of Iraq*; Scientific Press Ltd.: Beaconfield, 2010.

(22) Aqrawi, A. A. M.; Goff, J. C.; Horbury, A. D.; Sadooni, F. N. *The Petroleum Geology of Iraq*; Scientific Press: Beaconsfield, 2010; pp 424.
(23) Sadooni, F. N.; Alsharhan, A. S. Stratigraphy, lithofacies distribution, and petroleum potential of the Triassic strata of the northern Arabian plate. *AAPG Bull.* **2004**, *88* (4), 515−538.
(24) Ali, S. A.; Nutman, A. P.; Aswad, K. J.; Jones, B. G. Overview of the tectonic evolution of the Iraqi Zagros thrust zone: sixty million years of Neotethyan ocean subduction. *J. Geodyn.* **2019**, *129*, 162−177.
(25) Asaad, I. S.; Omer, M. F. Facies characterization and depositional environment of Baluti Formation (Late Triassic) from selected sections in the Kurdistan region, Northern Iraq. *Arabian J. Geosci.* **2020**, *13*, 1253.
(26) Mackertich, D. s.; Samarrai, A. I. History of hydrocarbon exploration in the Kurdistan Region of Iraq. *GeoArabia* **2015**, *20*, 181−220.
(27) Buday, T. The regional geology of Iraq. *Stratigraphy and Palaergeography 1*; Publications of GEOSURV: Baghdad, 1980; p 445.
(28) Peters, K.; Cassa, M. Applied Source Rock Geochemistry. In *The Petroleum System from Source to Trap*; Magoon, L. B., Dow, W. G., Eds.; American Association of Petroleum Geologists Memory, 1994; Vol. *60*, pp 93−117.
(29) Teichmüller, M. The origin of organic matter in sedimentary rocks. In *Organic petrology*; Taylor, G. H., Teicmüller, M., Davis, A., Diessel, C. F. K., Littke, R., Robert, P., Eds.; Gebrüder Borntraeger: Berlin, 1998; p 704.
(30) ASTM. 2004 ASTM C856−04 (2004). Standard Practice for Petrographic Examination of Hardened Concrete. *Annual Book of ASTM Standards*; American Society for Testing and Materials West Conshohocken: PA, 2004.
(31) Philp, R. P. Biological markers in fossil fuel production. *Mass Spectrom. Rev.* **1985**, *4*, 1−54.
(32) Peters, K. E.; Walters, C. C.; Moldowan, J. M. *The Biomarker Guide*, 2nd ed.; Cambridge University Press: Cambridge, UK., 2005; p 1155.
(33) Hakimi, M. H.; Abdullah, W. H.; Shalaby, M. R. Molecular composition and organic petrographic characterization of Madbi source rocks from the Kharir Oilfield of the Masila Basin (Yemen): palaeoenvironmental and maturity interpretation. *Arab. J. Geosci.* **2012**, *5*, 817−831.
(34) Van Bellen, R. C.; Dunnington, H. V.; Wetzel, R.; Morton, D. M. *Lexique Stratigraphic International, Paris, v. III, Asie, Fascicule 10a Iraq*; Centre National de la Recherche Scientifique, 1959; p 333.
(35) Lunn, G. A.; Miller, S.; Samarrai, A. Dating and correlation of the Baluti Formation, Kurdistan, Iraq: Implications for the regional recognition of a Carnian "marker dolomite" and a review of the Triassic to Early Jurassic sequence stratigraphy of the Arabian Plate. *J. Petrol. Geol.* **2019**, *42* (1), 5−36.
(36) Mohialdeen, I. M. J.; Fatah, S. S.; Abdula, R. A.; Hakimi, M. H.; Abdullah, W. H.; Khanaqa, P. A.; Lunn, G. A. Stratigraphic correlation and source rock characteristics of the Baluti Formation from selected wells in the Zagros Fold Belt of Kurdistan region, northern Iraq. *J. Petrol. Geol.* **2022**, *45* (1), 29−56.
(37) Hakimi, M. H.; Abdullah, W. H. Thermal maturity history and petroleum generation modelling for the Upper Jurassic Madbi source rocks in the Marib-Shabowah Basin, western Yemen. *Mar. Petrol. Geol.* **2015**, *59*, 202−216.
(38) Hadad, Y. T.; Hakimi, M. H.; Abdullah, W. H.; Makeen, Y. M. Basin modeling of the late Miocene Zeit source rock in the Sudanese portion of red sea basin: implication for hydrocarbon generation and expulsion history. *Mar. Petrol. Geol.* **2017**, *84*, 311−322.
(39) Qadri, S. M. T.; Shalaby, M. R.; Islam, M. A.; Hoon, L. L. Source rock characterization and hydrocarbon generation modeling of the Middle to Late Eocene Mangahewa Formation in Taranaki Basin, New Zealand. *Arabian J. Geosci.* **2016**, *9*, 559.
(40) Makeen, Y. M.; Abdullah, W. H.; Pearson, M. J.; Hakimi, M. H.; Elhassan, O. M. A.; Hadad, Y. T. Thermal maturity history and petroleum generation modelling for the lower cretaceous Abu Gabra formation in the Fula sub-basin, Muglad Basin, Sudan. *Mar. Pet. Geol.* **2016**, *75*, 310−324.
(41) Abdula, R. A. Oil and gas generation history based on burial history reconstruction and thermal maturity modeling of petroleum systems in Kurdistan Region, Iraq. *J. Zankoi Sulaimani* **2016**. (in press).
(42) Lachenbruch, A. Crustal temperature and heat production: Implications of the linear heat-flow relation. *J. Geophys. Res.* **1970**, *75*, 3291−3300.
(43) He, S.; Middleton, M. Heat flow and thermal maturity modelling in the northern carnarvon basin, north west shelf, Australia. *Mar. Petrol. Geol.* **2002**, *19*, 1073−1088.
(44) Li, M. J.; Wang, T. G.; Chen, J. F.; He, F. Q.; Yun, L.; Akbar, S.; Zhang, W. B. Paleo heat flow evolution of the Tabei Uplift in Tarim basin, northwest China. *J. Asian Earth Sci.* **2010**, *37*, 52−66.
(45) Welte, D. H.; Horsfield, B.; Baker, D. R. *Petroleum and Basin Evolution: Insights from Petroleum Geochemistry, Geology and Basin Modeling*; Springer: Berlin Heidelberg, 2012.
(46) Shalaby, M. R.; Hakimi, M. H.; Abdullah, W. H. Geochemical characteristics and hydrocarbon generation modeling of the Jurassic source rocks in the Shoushan Basin, north Western Desert, Egypt. *Mar. Petrol. Geol.* **2011**, *28*, 1611−1624.
(47) Shalaby, M. R.; Hakimi, M. H.; Abdullah, W. H. Modeling of gas generation from the Alam El-Bueib Formation in the Shoushan basin, northern western desert of Egypt. *Int. J. Earth Sci.* **2013**, *102*, 319−332.
(48) Allen, P. A.; Allen, T. R. *Basin Analysis: Principles and Applications*; Blackwell Scientific publications: Oxford, 1990.
(49) Allen, P. A.; Allen, J. R. *Basin Analysis: Principles and Applications*; Blackwell, Oxford, 2005; p 549.
(50) Hantschel, T.; Kauerauf, A. I. *Fundamentals of Basin and Petroleum Systems Modeling: Integrated Exploration Systems GmbH*; Schlumberger Company, Springer- Verlag Berlin Heidelberg, 2009.
(51) Waples, D. W. Time and temperature in petroleum formation: application of Lopatin's method to petroleum exploration. *AAPG Bull.* **1980**, *64*, 916−926.
(52) Sweeney, J. J.; Burnham, A. K. Evaluation of a simple model of vitrinite reflectance based on chemical kinetics. *Am. Assoc. Pet. Geol. Bull.* **1990**, *74*, 1559−1570.
(53) Jarvie, D. M.; Claxton, B. L.; Henk, F.; Breyer, J. T. Oil and shale gas from the Barnett Shale, Ft. *AAPG Annual Meeting Program*: Worth Basin, Texas (Abs.), 2001; p A100.
(54) Katz, B.; Lin, F. Consideration of the limitations of thermal maturity with respect to vitrinite reflectance, Tmax, and other proxies. *AAPG* **2021**, *105*, 695−720.
(55) Clark, J. P.; Philp, R. P. Geochemical Characterization of Evaporite and Carbonate Depositional Environments and Correlation of Associated Crude Oils in the Black Creek Basin, Alberta. *Bull. Can. Petrol. Geol.* **1989**, *37*, 401−416.
(56) Chakhmakhchev, A.; Suzuki, M.; Takayama, K. Distribution of alkylated dibenzothiophenes in petroleum as a tool for maturity assessments. *Org. Geochem.* **1997**, *26*, 483−489.
(57) Radke, M.; Welte, D. H. The methylphenanthrene index (MPI): a maturity parameter based on aromatic hydrocarbons. *Adv. Org. Geochem.* **1981**, *1983*, 504−512. Bjory, M. (Ed.)
(58) Pu, F.; Philip, R.; Zhenxi, L.; Guangguo, Y. Geochemical characteristics of aromatic hydrocarbons of crude oils and source rocks from different sedimentary environments. *Org. Geochem.* **1990**, *16*, 427−435.
(59) Hughes, W. B.; Holba, A. G.; Dzou, L. I. P. The Ratios of Dibenzothiophene to Phenanthrene and Pristane to Phytane as Indicators of Depositional Environment and Lithology of Petroleum Source Rocks. *Geochim. Cosmochim. Acta* **1995**, *59*, 3581−3598.
(60) Radke, M.; Vriend, S. P.; Ramanampisoa, L. R. Alkyldibenzofurans in terrestrial rocks: Influence of organic facies and maturation. *Geochim. Cosmochim. Acta* **2000**, *64*, 275−286.
(61) Li, M.; Wang, T.; Zhong, N.; Zhang, W.; Sadik, A.; Li, H. Ternary diagram of fluorenes, dibenzothiophenes and dibenzofurans: Indicating depositional environment of crude oil source rocks. *Energy Explor. Exploit.* **2013**, *31*, 569−588.
(62) Asif, M.; Wenger, L. M. Heterocyclic aromatic hydrocarbon distributions in petroleum: A source facies assessment tool. *Org. Geochem.* **2019**, *137*, 103896.

https://doi.org/10.1021/acsomega.3c09003
ACS Omega 2024, 9, 7085−7107

(63) Chen, S.; Zhu, Y.; Wang, H.; Liu, H.; Wei, W.; Fang, J. Shale gas reservoir characterisation: A typical case in the southern Sichuan Basin of China. *Energy* **2011**, *36*, 6609−6616.
(64) Jarvie, D. M.; Hill, R. J.; Ruble, T. E.; Pollastro, R. M. Unconventional shale-gas systems: The Mississippian Barnett Shale of north-central Texas as one model for thermogenic shale-gas assessment. *Am. Assoc. Pet. Geol. Bull.* **2007**, *91*, 475−499.
(65) Wang, F. P.; Gale, J. F. W. Screening criteria for shale-gas systems. *Gulf Coast Assoc. Geol. Soc. Trans.* **2009**, *59*, 779.
(66) Mohamed, A. Y.; Whiteman, A. J.; Archer, S. G.; Bowden, S. A. Thermal modelling of the Melut basin Sudan and South Sudan: Implications for hydrocarbon generation and migration. *Mar. Petrol. Geol.* **2016**, *77*, 746−762.
(67) Botor, D.; Bábek, O. Burial and thermal history modelling of the Upper Carboniferous strata based on vitrinite reflectance data from Bzie-Dębina-60 borehole (Upper Silesian Coal Basin, southern Poland). *Geologické výzkumy na Moravě a ve Slezsku* **2019**, *26*, 73−79.
(68) Ameen, M. S. Possible forced folding in the Taurus-Zagros belt of northern Iraq. *Geol. Mag.* **1991**, *128*, 561−584.
(69) Berberian, M. Master "blind" thrust faults hidden under the Zagros folds: active basement tectonics and surface morphotectonics. *Tectonophysics* **1995**, *241*, 193−224.
(70) Hessami, K.; Koyi, H. A.; Talbot, C. J.; Tabasi, H.; Shabanian, E. Progressive unconformities within an evolving foreland fold−thrust belt, Zagros Mountains. *J. Geol. Soc. Lond* **2001**, *158*, 969−981.
(71) Sherkati, S.; Letouzey, J. Variation of structural style and basin evolution in the central Zagros (Izeh zone and Dezful Embayment), Iran. *Iran. Mar. Pet. Geol.* **2004**, *21*, 535−554.
(72) Agard, P.; Omrani, J.; Jolivet, L.; White church, H.; Vrielynck, B.; Spakman, W.; Monie, P.; Meyer, B.; Wortel, R. Zagros Orogeny: a subduction-dominated process. *Geol. Mag.* **2011**, *148*, 692−725.
(73) Allen, M. B.; Saville, C.; Blanc, E. J.-P.; Talebian, M.; Nissen, N. Orogenic plateau growth: expansion of the Turkish-Iranian Plateau across the Zagros folds-and thrust belt. *Tectonic* **2013**, *32*, 171.
(74) Hadad, Y. T.; Hakimi, M. H.; Abdullah, W. H.; Kinawy, M.; El Mahdy, O.; Lashin, A. Organic geochemical characteristics of Zeit source rock from Red Sea Basin and their contribution to organic matter enrichment and hydrocarbon generation potential. *J. African Earth Sci.* **2021**, *177*, 104151.
(75) Zumberge, J. E. Terpenoid biomarker distributions in low maturity crude oils. *Org. Geochem.* **1987**, *11*, 479−496.
(76) Waples, D.; Machihara, T. *Biomarkers for Geologists: A Practical Guide to the Application of Steranes and Triterpanes in Petroleum Geology, Methods in Exploration Series*; American Association of Petroleum Geologists, 1991.
(77) Murray, A. P.; Boreham, C. J. *Organic Geochemistry in Petroleum Exploration*; Aust. Geol. Surv. Organ. Canberra, 1992; p 230.
(78) Bray, E. E.; Evans, E. D. Distribution of n-paraffins as a clue to recognition of source beds. *Geochim. Cosmochim. Acta* **1961**, *22*, 2−15.
(79) Connan, J.; Cassou, A. M. Properties of gases and petroleum liquids derived from terrestrial kerogen at various maturation levels. *Geochim. Cosmochim. Acta* **1980**, *44*, 1−23.
(80) Didyk, B. M.; Simoneit, B. R. T.; Brassell, S. C. t.; Eglinton, G. Organic geochemical indicators of palaeoenvironmental conditions of sedimentation. *Nature* **1978**, *272*, 216−222.
(81) Chandra, K.; Mishra, C. S.; Samanta, U.; Gupta, A.; Mehrotra, K. L. Correlation of different maturity parameters in the Ahmedabad-Mehsana block of the Cambay basin. *Org. Geochem.* **1994**, *21*, 313−321.
(82) Huang, W. Y.; Meinschein, W. G. Sterols as ecological indicators. *Geochim. Cosmochim. Ac* **1979**, *43*, 739−745.
(83) Strachan, M. G.; Alexander, R.; Kagi, R. I. Trimethylnaphthalenes in crude oils and sediments: Effects of source and maturity. *Geochim. Cosmochim. Acta* **1988**, *52*, 1255−1264.
(84) Armstroff, A.; Wilkes, H.; Schwarzbauer, J.; Littke, R.; Horsfield, B. Aromatic hydrocarbon biomarkers in terrestrial organic matter of Devonian to Permian age. *Palaeogeog. Palaeoclimatol. Palaeoecol.* **2006**, *240*, 253−274.
(85) Bissada, K. K. Geochemical constraints on petroleum generation and migration—a review. *Proc. ASCOPE* **1982**, *81*, 69−87.
(86) Katz, B.; Lin, F. Lacustrine basin unconventional resource plays: Key differences. *Mar. Pet. Geol.* **2014**, *56*, 255−265.
(87) Jarvie, D. M. *Shale Resource Systems for Oil and Gas: Part 2-Shale-Oil Resource Systems*; American Association of Petroleum Geologists, 2012.
(88) Hu, T.; Pang, X.; Wang, Q.; Jiang, S.; Wang, X.; Huang, C.; Xu, Y.; Li, L.; Li, H. Geochemical and geological characteristics of Permian Lucaogou Formation shale of the well Ji174, Jimusar Sag, Junggar Basin, China: Implications for shale oil exploration. *Geol. J.* **2018**, *53*, 2371−2385.
(89) Shalaby, M. R.; Hakimi, M. H.; Abdullah, W. H. Geochemical characterization of solid bitumen (migrabitumen) in the Jurassic sandstone reservoir of the Tut Field, Shushan Basin, northern Western Desert of Egypt. *Int. J. Coal Geol.* **2012**, *100*, 26−39.
(90) Seifert, W. K.; Michael Moldowan, J. The effect of biodegradation on steranes and terpanes in crude oils. *Geochim. Cosmochim. Acta* **1979**, *43*, 111−126.
(91) Seifert, W. K.; Moldowan, J. M. Paleoreconstruction by biological markers. *Geochim. Cosmochim. Acta* **1981**, *45*, 783.
(92) Seifert, W. K.; Moldowan, J. M. Use of biological markers in petroleum exploration. In *Methods in Geochemistry and Geophysics Book*; Johns, R. B., Ed.; Amsterdam Series, 1986; Vol. *24*, pp 261−290.
(93) Mackenzie, A. S.; Patience, R. L.; Maxwell, J. R.; Vandenbroucke, M.; Durand, B. Molecular parameters of maturation in the Toarcian shales, Paris Basin, France—I. Changes in the configurations of acyclic isoprenoid alkanes, steranes and triterpanes. *Geochim. Cosmochim. Acta* **1980**, *44*, 1709−1721.
(94) Behar, F.; Vandenbroucke, M.; Tang, Y.; Marquis, F.; Espitalie, J. Thermal cracking of kerogen in open and closed systems: determination of kinetic parameters and stoichiometric coefficients for oil and gas generation. *Org. Geochem.* **1997**, *26*, 321−339.

https://doi.org/10.1021/acsomega.3c09003
ACS Omega 2024, 9, 7085−7107